scientific reports

Check for updates

OPEN

Electrochemical and computational investigation of *Tinospora cordifolia* fractions as a novel corrosion inhibitor for carbon steel in seawater medium

Ahmad Royani[1]✉, Muhammad Hanafi[2], Abhinay Thakur[3], Abdelkader Zarrouk[4], Nabisab Mujawar Mubarak[5]✉ & Azwar Manaf[6]✉

This study employed electrochemical techniques and computational analyses to evaluate the efficacy of *Tinospora cordifolia* fraction (TCF) as an anticorrosion agent for carbon steel in a seawater medium. Electrochemical methods were employed to investigate the corrosion performance of carbon steel with and without TCF at different concentrations (25 to 150 mg.L^{-1}) and temperatures (300 K to 320 K). The findings revealed that TCF significantly decreased the corrosion current density, exhibiting its efficacy as a corrosion inhibitor. The inhibition efficiency increases with the concentration of TCF and decreases with rising temperature. The most excellent value of efficiency inhibition corrosion based on concentration is around 90.89% (PDP) and 92.25% (EIS) with the addition of 150 mg.L^{-1} of TCF. The temperature dependence of the inhibitor efficiency shows that its performance decreases slightly (from 90.89% to 83.74%) with increasing temperature (from 300 to 320 K), but remains effective even at high temperatures. The inhibitor exhibited a mixed-type inhibitory mechanism, although it tends to reduce the cathode oxygen reaction (cathodic-type). Adsorption studies revealed that bioactive compounds from TCF adhered to the steel surface, following the Langmuir isotherm, with a negative free energy value (ΔG_{ads} = − 26.73 kJ/mol at 300 K), indicating spontaneous adsorption. Computational analyses with density functional theory (DFT) confirmed the molecular interactions between moupinamide (the dominant active substance in TCF) and the steel surface in corrosion inhibition. This study highlights the effectiveness of TCF as a corrosion inhibitor and elucidates its inhibition mechanism, sorption behaviour, and fundamental molecular interactions.

Keywords Carbon steel, Green inhibitor, Plant extract, Seawater, *Tinospora*

Corrosion of metals, mainly carbon steel, in marine environments is a significant problem that causes material degradation, economic losses, and environmental damage. With its high chloride content, seawater acts as a highly corrosive medium for steel and other metallic materials, necessitating the use of corrosion inhibitors to mitigate these effects. Corrosion inhibitors were often applied to protect steel surfaces from aggressive attacks, thereby mitigating steel degradation[1]. Conventional corrosion inhibitors are usually synthetic chemicals that, although effective, raise concerns regarding toxicity and environmental sustainability[2]. Therefore, there is

[1]Central Laboratory for Corrosion Studies and Mitigation Technology, Research Center for Metallurgy, National Research and Innovation Agency–BRIN, KST B. J. Habibie 225 Buildings, Puspiptek Area, South Tangerang, Banten 15314, Indonesia. [2]Research Center for Pharmaceutical Ingredients and Traditional Medicine, National Research and Innovation Agency–BRIN, KST Soekarno, Jl. Raya Jakarta-Bogor KM. 46, Cibinong, West Java 16911, Indonesia. [3]Division of Research and Development, Lovely Professional University, Phagwara, Punjab, India. [4]Laboratory of Materials, Nanotechnology and Environment, Faculty of Sciences, Mohammed V University in Rabat, Av. Ibn Battouta, P.O.Box, 1014, Agdal-Rabat, Morocco. [5]Department of Chemical Engineering, College of Engineering, Imam Mohammad Ibn Saud Islamic University (IMSIU), Riyadh 11432, Saudi Arabia. [6]Postgraduate Program of Materials Science Study, Department of Physics, Faculty of Mathematics and Natural Sciences, Universitas Indonesia, Depok 16424, Indonesia. ✉email: ahmad.royani@brin.go.id; MNSMujawar@imamu.edu.sa; azwar@sci.ui.ac.id

increasing interest in developing environmentally friendly and sustainable corrosion inhibitors derived from natural sources. Among the various classes of inhibitors, organic or natural compounds with heteroatoms, such as sulfur, nitrogen, and oxygen, have shown promising results due to their ability to inhibit metal surfaces through adsorption, forming a protective layer that reduces corrosion[3,4]. These inhibitors typically contain functional groups such as amines, imidazoles, thiols, and other heteroatoms that can adsorb onto metal surfaces, resulting in a protective film that isolates the metal from aggressive ions[5]. Adsorption inhibitors can be either physisorption or chemisorption, with the latter involving stronger chemical bonds[6].

Plant-based inhibitors have gained prominence due to their availability, low cost, and environmentally friendly nature[7]. Several studies have identified various plant extracts that exhibit corrosion-inhibitory properties, such as those from *Nepeta cataria L.* with efficiency from 91.24% to 90.05% for 25 °C to 35 °C at 800 mg.L^{-1}[8], *Nigella sativa L.* with inhibition effectiveness of 94% at 600 ppm[9], *glucomannan* with 98.8% at 0.5 mmol.L^{-1}[10], and *anthocleista grandiflora* with 92.4% at 800 ppm in seawater[11]. These natural inhibitors usually contain alkaloids, flavonoids, and tannins, which interact with the metal surface to form a protective layer, thereby reducing the corrosion rate[12,13]. However, the effectiveness of these inhibitors in complex media such as seawater and NaCl is inconsistent[14,15], necessitating further research on their performance under real-world conditions. The effectiveness of corrosion inhibitors is often evaluated using electrochemical techniques, such as potentiodynamic polarization[16], electrochemical impedance spectroscopy (EIS)[17], and weight loss methods[18]. Computational studies using quantum chemical calculations also play a vital role in understanding the molecular mechanisms behind the corrosion inhibition process, offering insights into the interactions between inhibitor molecules and metal surfaces[19,20].

Tinospora cordifolia, a medicinal plant known for its bioactive properties, has shown promise in various pharmacological applications[21–25]. However, its potential as a corrosion inhibitor, especially for carbon steel in seawater, remains unexplored. Previous studies have shown that *Tinospora* extracts can effectively control corrosion by adsorption onto the steel surface and producing a protective film that reduces electrochemical activity in chloride acid[26] and artificial seawater[27]. The inhibition effectiveness of *Tinospora crispa* extract was found to be 78.14% (PDP) and 81.58% (EIS) at a dosage of 800 ppm for mild steel metal in 1 mol.L^{-1} HCl[26]. Meanwhile, the inhibitory effectiveness of *Tinospora cordifolia* extract (300 ppm) in artificial seawater for mild steel was 85.94% at 310 K[27]. Although the corrosion inhibition ability of *Tinospora* extract has been well documented, the concentration dose used is still relatively high and is still in the form of crude extract. Therefore, the effectiveness of *Tinospora cordifolia* derivatives (fractions), especially in seawater solution media, remains an interesting field of study and warrants further development.

This study aimed to investigate the corrosion inhibition efficiency of the active fraction of *Tinospora cordifolia extract (TCF)* on carbon steel in seawater, focusing on the effects of TCF concentration and temperature of the medium. In addition, this study aimed to analyze the adsorption mechanism of TCF onto steel surfaces using Langmuir adsorption isotherms and to evaluate its thermodynamic performance. The corrosion inhibition efficiency of TCF for carbon steel in seawater was evaluated using electrochemical techniques, including potentiodynamic polarization (PDP), electrochemical impedance spectroscopy (EIS), and a computational approach. Surface morphology analysis was performed using SEM–EDS, AFM, and XPS. The novelty of this study lies in the use of bioactive green inhibitors, specifically the active fraction of *Tinospora* extract, as several previous studies have employed crude extracts. In addition, its comprehensive approach combines experimental and computational electrochemical analysis to evaluate the performance of TCF as an anticorrosion agent for carbon steel in seawater environments. The combination of electrochemical techniques and computational modelling provides an opportunity to gain a more comprehensive understanding of the inhibitor's performance, adsorption process, and nature of the corrosion inhibition mechanism, which has not been previously reported for *Tinospora cordifolia* fractions. Therefore, this study aims to evaluate TCF as a corrosion inhibitor and provide a deeper understanding of the complex relationships between organic inhibitors and metal surfaces, thereby contributing to the development of more effective corrosion control solutions in industrial applications.

Experimental

Material

Carbon steel specimens from the geothermal industry were used as substrate materials. The nominal chemical composition of the steel (wt.% %) by optical emission spectroscopy (Spark OES) was tabulated in Table 1. Salt powder (Marine Art, SF-1) was used as a simulated seawater solution representing the corrosive medium. This study utilized TCF as a novel corrosion inhibitor derived from *Tinospora cordifolia* leaf extracts. *T. cordifolia* plants were obtained from Balai Penelitian Tanaman Rempah dan Obat (Balittro), Bogor—West Java. Biovia Materials Studio software for density functional theory (DFT) analysis was used to model the interaction of corrosion inhibitors with the carbon steel surface.

Preparation

Carbon steel surface preparation

Carbon steel was cut to have an area of 1 cm^2. Carbon steel was linked to copper wire for electrochemical investigations and mounted using epoxy glue. Before the tests, the working electrode surface had been ground

Element	C	Mn	Si	Ni	S	Cr	Al	Cu	P	Fe
Content (wt.% %)	0.18	1.27	0.26	0.011	<0.005	0.035	0.022	0.011	0.0031	Balance

Table 1. The nominal chemical composition of carbon steel was utilized in this study.

and polished with abrasion paper grades (SiC) ranging from 60 to 1200 mesh. After that, it was cleaned with acetone and methanol to remove the fat, in accordance with ASTM G-5 and G-31 standards.

Seawater medium preparation
Seawater medium was prepared by following ASTM D1141. 3.8 g of salt powder (Mrine Art SF-1) was diluted in 1 L of distilled water to generate the solution media. Meanwhile, the inhibitor was added to seawater medium at varying concentrations (25 mg.L^{-1} to 150 mg.L^{-1}) for electrochemical studies. The concentration was determined by dissolving the solid from the filtrate to form a stock solution, and then diluting it in the test solution. A control group without the extract was also tested.

TCF preparation
Fresh *Tinospora cordifolia* leaves are cleaned, dried, and then ground into a fine powder. The *Tinospora cordifolia* powder is subjected to extraction using 50% methanol (volume) to isolate fractions containing various phytochemicals. After extraction, the solvent is evaporated (50 °C), and the residues are fractioned using column chromatography with hexane, ethyl acetate, and methanol. In this work, the solid fraction resulting from a hexane:ethyl acetate (2:1) mixture is used to inhibit the corrosion of carbon steel in a seawater medium.

Phytosubstance characterization
UV–Vis (UH5300 Spectrophotometer), FT-IR (Bruker-Tensor II), HR-MS (Thermo Scientific Orbitrap Exploris 120), and NMR (JEOL JNM-ECX500 MHz) were used to identify and confirm the active compounds in the TCFs. The fractions were dissolved in ethanol to achieve a concentration of 100 µg/mL for UV–Vis analysis. The sample was placed in a quartz cuvette and scanned (400 nm.min^{-1}) in the spectrum with the UV–Vis range (1000–200 nm). FT-IR characterization was performed in the wavelength range of 4000 to 500 cm^{-1}, with 45 sample scans. HR-MS measurement was performed using a ZORBAX Eclipse Plus C18RRHD column (2.1 mm × 100 mm, 1.8 µm) in the mass range of 100–700 m/z with an injection volume of 10 µL. Furthermore, FT-NMR was performed using CD_3OD solvent with ^{1}H-NMR, ^{13}C-NMR, and 2D-NMR techniques.

Electrochemical study

A standard three-electrode cell system is utilized for electrochemical experiments. The working electrode was a carbon steel coupon with an open area of 1 cm^2. A saturated calomel electrode (SCE) served as the reference electrode to maintain a stable potential, while a platinum plate functioned as the counter electrode, completing the circuit. This study involved electrochemical experiments conducted with a potentiostat (Gamry G750-50,090 model).

OCP study
An open-circuit potential (OCP) measurement was performed to determine the potential prior to the electrochemical measurement. The OCP was carried out with a 0.5 sample period for 600 s for each medium temperature.

PDP study
Potentiodynamic polarization (PDP) evaluations were performed to determine the corrosion current density (I_{corr}) and the Tafel slope for both the cathode and anode. After stabilization of the OCP for 600 s, the potentiodynamic polarization was examined at a rate of 1 mV/s between − 250 mV and + 250 mV relative to the OCP. The linear cross-sections of the anode and cathode curves were extrapolated to determine the corrosion parameters, such as I_{corr}, E_{corr}, and slope. The PDP inhibition efficiency was determined by using Eq. 1 [28], where $(I_{corr})_0$ and $(I_{corr})_1$ represent the corrosion currents in the absence and the presence of inhibitors (µA.cm^{-2}):

$$\%IE = \frac{(i_{corr})_o - (i_{corr})_1}{(i_{corr})_o} \times 100 \tag{1}$$

EIS Study
Electrochemical impedance spectroscopy (EIS) was performed with an amplitude of 10 mV per decade over a frequency range of 5 × 10^4 Hz to 10^ (− 1) Hz. The charge transfer resistance (R_{ct}) and double layer (C_{dl}) were determined by fitting the result curves to a suitable circuit model.

The corrosion inhibition efficiency was calculated from the change in polarisation resistance R_p using the formula as follows in Eq. (2) [29]:

$$\eta\,(\%) = \left(1 - \frac{R_{p0}}{R_{p1}}\right) \times 100 \tag{2}$$

$$R_p = R_{ct} + R_f \tag{3}$$

In this equation, Rct is the charge transfer resistance, Rf is the resistance of the film, and Rp0 and Rp1 denote the resistance polarisation without and with TCF, respectively, as act inhibitors.

Surface analysis

The scanning electron microscope (SEM, JEOL JSM IT100) coupled with EDX was used to characterize the differences in morphologies between the extracted and carbon steel surfaces. For carbon steel samples, morphology photos were taken at 300 K after submerging them in a seawater medium for 24 h, both with and

without the presence of 150 mg.L^{-1} TCF. The topography and morphology of the carbon steel surface were characterized using atomic force microscopy (AFM, Park NX10). X-ray Photoelectron Spectroscopy (XPS, Kratos Axis Supra^{+}) was employed to investigate the chemical composition and oxidation states of the elements on the surface of the samples.

Computation study

Density functional theory (DFT) was employed to calculate the electronic properties of the inhibitor molecules and their potential for adsorption onto the carbon steel surface. Theoretical analysis of the dominant bioactive TCF (moupinamide) was performed using the Dmol^3 module within the Biovia Materials Studio software suite 2020 and Gauss View 6.0.16[30]. The selection of the Double Numerical plus d-functions (DNP) basis set was intentional, aimed at precisely capturing the molecular structure and electronic characteristics. The Perdew-Burke-Ernzerhof (PBE) generalized gradient approximation was applied to determine the exchange–correlation energy, and COSMO (water + NaCl) to obtain capture solvation effects. In this study, the convergence conditions for the ionic calculations were set to approximately 2.7 × 10^ (− 4) eV for the energy change, 0.054 eV/Å for the force change, and a density mode was used to improve geometry convergence. Several quantum chemical parameters like electronegativity (χ), electronic affinity (A), global hardness (η), softness (σ), ionization potential (I), E_{LUMO}, and E_{HOMO} were calculated using Eq. (4) to Eq. (10) to determine the reactivity of the molecule[31].

$$\Delta E = E_{HOMO} - E_{LUMO} \tag{4}$$

$$I = -E_{HOMO} \tag{5}$$

$$A = -E_{LUMO} \tag{6}$$

$$\eta = \left(\frac{I - A}{2}\right) \tag{7}$$

$$\chi = \left(\frac{I + A}{2}\right) \tag{8}$$

$$\sigma = \frac{1}{\eta} \tag{9}$$

$$\Delta N = \frac{\chi_{Fe} - \chi_{Inh}}{2\left(\eta_{Fe} - \eta_{inh}\right)} \tag{10}$$

Here, ηinh and χinh represent the molecule's hardness and electronegativity, respectively. To calculate ΔN, the parameters Φfe (110) = 4.82 eV and ηFe (110) = 0 eV were utilized.

Results and discussion

Phytosubstances of TCF

UV–Vis characteristics

The results of the UV–Vis spectrum of the TCF are shown in Fig. 1. The spectrum of the TCF shows several absorbance peaks in the range of 260–550 nm. The bands at 260 nm and 308 nm indicate the presence of alkaloid and tannin compounds, respectively. Phenolic compounds are seen at the peak of the 348 nm band due to their aromatic hydroxyl groups. Flavonoid compounds are detected at an absorption of around 384 nm due to the presence of a conjugated ring structure. Furthermore, the peak range of 422 nm to 528 nm is considered characteristic of chlorophyll compounds. This chlorophyll absorbance band aligns with the findings reported in the ethanol extraction of *Dillenia suffruticosa* leaves[32].

FT-IR characteristics

FT-IR (Fourier Transform Infrared Spectroscopy) analysis was employed to identify the functional groups present in compounds contained in the TCF, as well as to elucidate the chemical structure of active compounds that may contribute to the corrosion inhibition of carbon steel in seawater media. The results of the TCF spectra measurements are shown in Fig. 2**.**

The wide band in the valley (3300–3350 cm^1) indicates the presence of hydroxyl groups (O–H groups). This band is a characteristic of polyphenol, flavonoid, or tannin compounds that have the potential to be corrosion inhibitors by forming a protective layer on the surface of carbon steel. The C–H group was identified at 2800–3000 cm^1, and this band indicates the presence of alkyl compounds or compounds with alkyl groups in the structure. In addition, a carbonyl group (C=O) at 1704 cm^{-1} was also detected, which can interact with the surface of carbon steel through the adsorption process. In TCF, double bonds in aromatic compounds, such as flavonoids or polyphenols, were also detected in the band 1600 cm^{-1}. Furthermore, in the band 1225 cm^{-1} (C–O group), it is suspected that the compound is an ester or phenolic compound, essential in increasing the metal surface's affinity and corrosion inhibition efficiency.

FT-IR analysis revealed that the TCF contains bioactive compounds, including phenols, flavonoids, and esters, which possess active functional groups such as –OH, C=O, and C=C, potentially playing a role in inhibiting the corrosion process in carbon steel. These compounds can potentially adsorb on the surface of carbon steel, forming a protective layer that reduces the interaction of the metal with corrosive media. Therefore, the active compounds in *Tinospora cordifolia* can effectively protect against corrosion, especially in seawater environments.

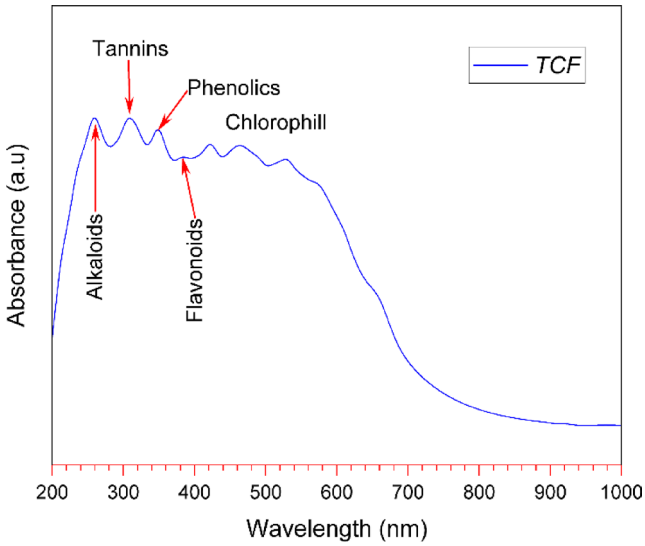

Fig. 1. UV–Vis spectra of *TCF*.

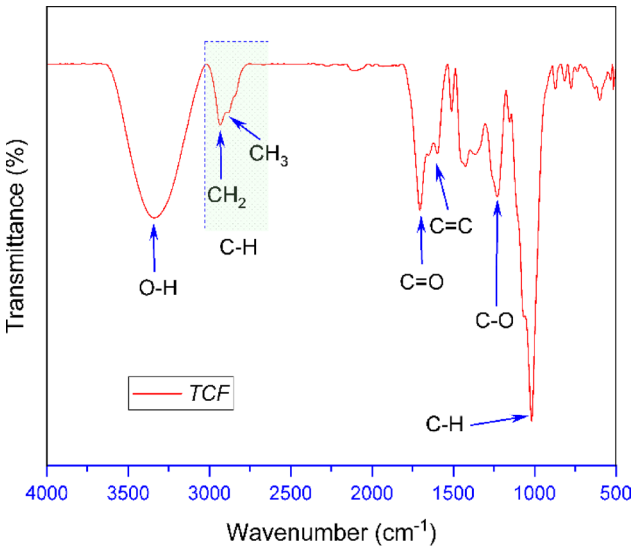

Fig. 2. FT-IR spectra of *TCF*.

HR-MS analysis

HR-MS (High-Resolution Mass Spectrometry) analysis was employed to determine the molecular weight and structure of compounds present in the TCF, as well as to identify bioactive compounds with the potential to act as corrosion inhibitors on carbon steel in seawater media. The results of the TCF spectra with HR-MS are shown in Fig. 3.

The spectral results in Fig. 3 show several peaks, with the prominent peak detected at m/z (mass-to-charge ratio) 314. This peak indicates a possible compound with a molecular weight of around 313 Da. Based on literature data, this may be related to flavonoids or phenolics, often found in *Tinospora cordifolia*[33]. There is also a peak at m/z 177, indicating a compound with a smaller structure, most likely a phenolic derivative or a flavonoid compound, which also contributes to the inhibition mechanism.

NMR analysis

The NMR results on the dominant compound of the TCF are shown in Fig. 4. Based on the results of specific H-NMR, C-NMR, and 2D-NMR spectra, this compound is suspected to be N-(4-Hydroxy-3-methoxy-E-cinnamoyl)-4-(2-aminoethyl)phenol, also known as 4-(2-aminoethyl) N-trans-feruloyltyramine and Moupinamide. This finding is reinforced by the HRMS results, where the compound with a molecular weight of 313 (moupinamide) is the dominant compound in the TCF.

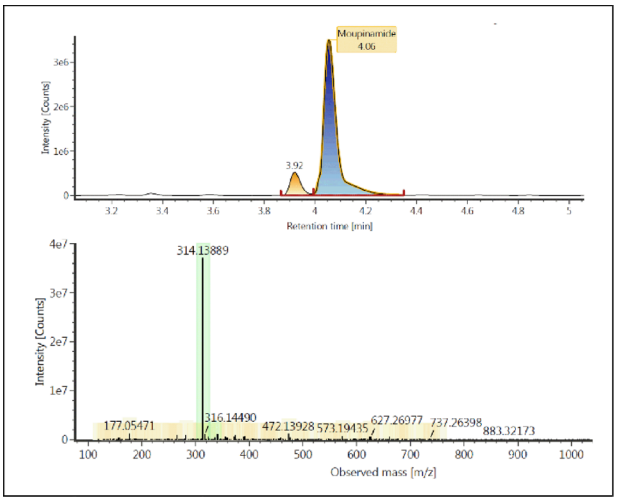

Fig. 3. HR-MS spectra of *TCF*.

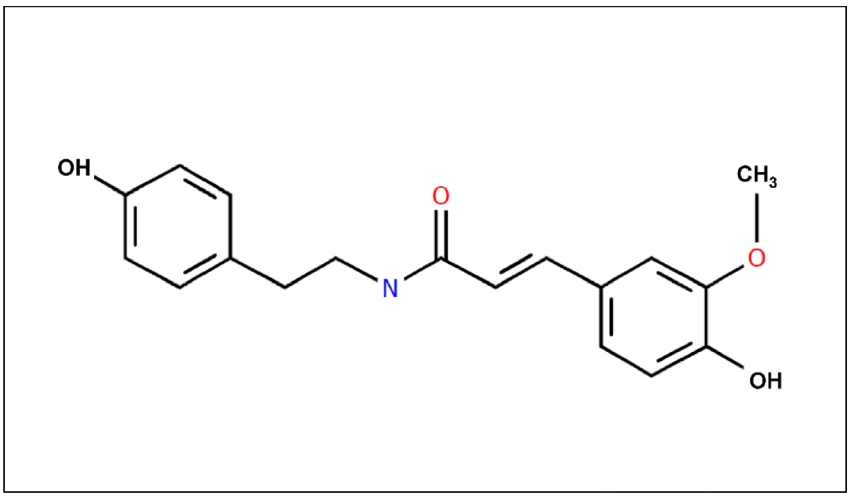

Fig. 4. NMR spectra of the compound from *TCF*.

Moupinamide can act as an inhibitory agent for corrosion activity on carbon steel in seawater media, considering that amide compounds often interact with metal surfaces[34]. The amide group (–CONH–) in Moupinamide can interact with metal surfaces through physical or chemical adsorption, forming a protective layer that reduces the interaction between metal and corrosive media. In addition, these compounds, especially those with amide and aromatic groups, can act as antioxidants, reducing oxidation reactions that occur on carbon steel in seawater media[35].

Electrochemical study

Open circuit potential (OCP) analysis

Open-circuit potential (OCP) measurements were performed to determine potential stability before applying the current. The results of the OCP graph for 600 s on carbon steel with and without *TCF* at various temperatures are presented in Fig. 5. The shift in the OCP value shifted negatively, indicating ongoing corrosion. However, in the presence of *TCF*, the OCP value stabilized over time, indicating the formation of a protective inhibitor layer on the steel surface. The stabilisation of the OCP over time further confirms the formation of a durable inhibitor layer that minimises the anodic and cathodic reactions responsible for corrosion. A limited range of potential shifts is − 606.9 mV to − 703.7 mV, − 612.9 mV to − 713.3 mV, and − 629.2 mV to − 727.7 mV for 300 K, 310 K, and 320 K, respectively. This limit of OCP may reflect the type of mixed inhibitors with cathode dominance[36].

On the other hand, it has been suggested that the shift towards more negative corrosion potentials is related to the absorption of inhibitors or desorption of corrosion products from the metal surface[37]. In addition, increasing temperature also causes a shift in the OCP value to be increasingly negative[38]. Similar behaviour also occurs in aloe saponaria extract[39], where the OCP moves negatively with the addition of extract.

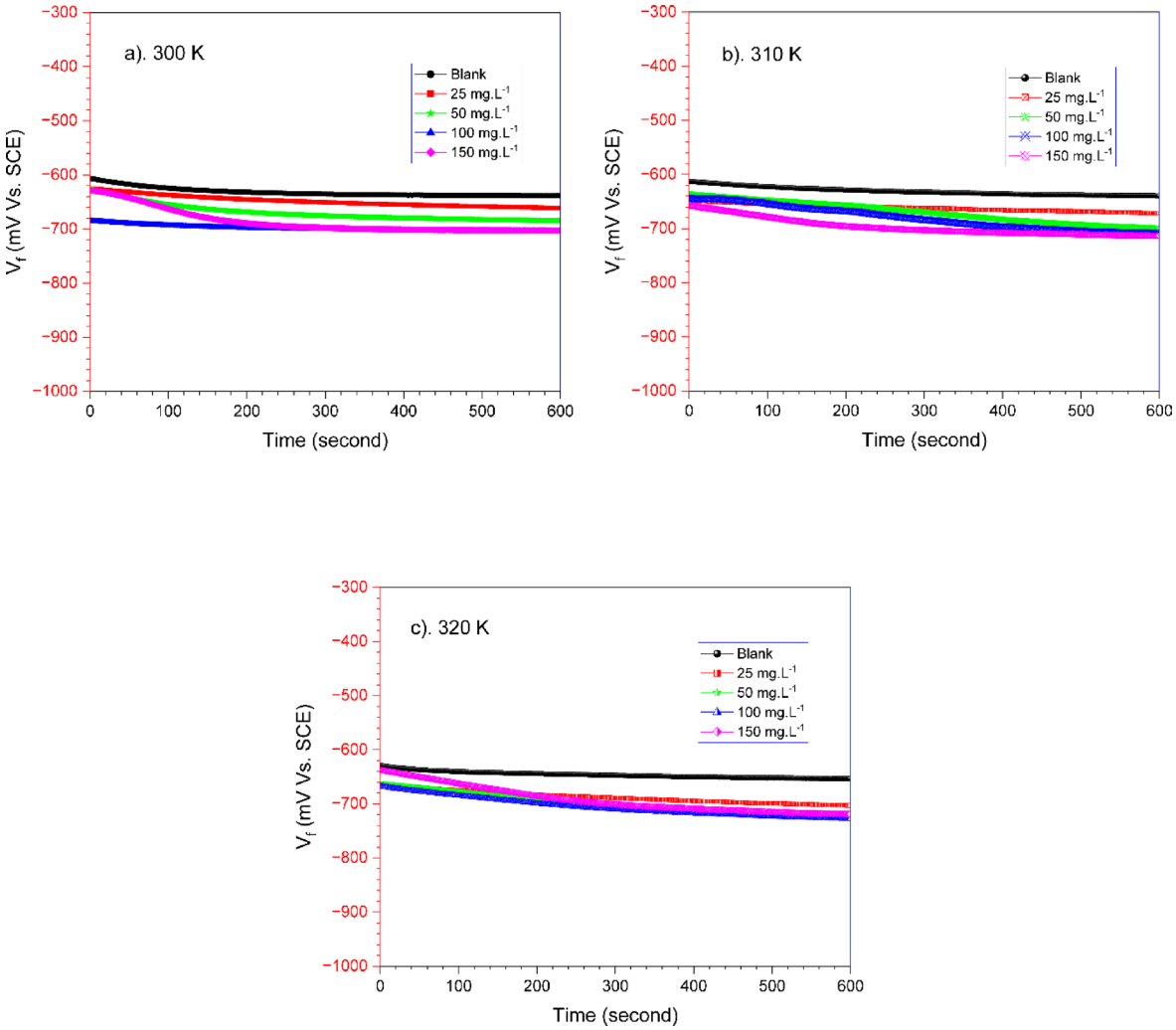

Fig. 5. Open circuit potential (OCP) curves of carbon steel in seawater with the absence and presence of varying TCF at (**a**) 300 K, (**b**) 310 K, and (**c**) 320 K.

Potentiodynamic polarization (PDP) analysis

The potentiodynamic polarization (PDP) measurements were conducted on carbon steel samples in a seawater medium with varying concentrations of TCF as an organic inhibitor, ranging from 25 to 150 mg.L^{-1}, at different temperatures. Polarization curves were recorded (Fig. 6), and key parameters involving corrosion current density (I_{corr}), Tafel slopes (β_c), and corrosion potential (E_{corr}) were extracted from the polarization plots as tabulated in Table 2. The PDP curve results show that the corrosion potential (E_{corr}) shifts toward negative values as the concentration of TCF increases. This decrease in corrosion potential indicates a tendency for the carbon steel surface to react with increasing concentrations of TCF[40]. The corrosion potential (E_{corr}) also shifts negatively with increasing temperature. This negative shift indicates that the activation energy for the corrosion process decreases, making the process more thermodynamically favorable and effortless to initiate at higher temperatures[41].

The cathodic slope (β_c) results in Fig. 6 provides information about the rate of oxygen reduction, which in this work tends to be cathodic inhibition. The β_c value changes with TCF, indicating a change in the cathode hydrogen evolution mechanism. This case suggests that the active substances in TCF significantly slow down carbon steel corrosion as their inhibition capacity increases with concentration. The β_c value changed slightly from 25 mg.L^{-1} to 100 mg.L^{-1}, indicating a minimal effect on the cathodic process. However, at a concentration of 150 mg.L^{-1}, β_c tended to increase, indicating that the inhibitor inhibited oxygen reduction, which is essential in reducing the corrosion rate[42]. The relatively unchanged Tafel slope (although slightly cathodic) suggests that the TCF does not alter the fundamental corrosion mechanism but instead reduces the overall rate of the anode and cathode processes[43]. This type of inhibition may be due to the chemical structure of the TCF molecule, which contains functional groups that can interact with metal surface atoms and reduce oxygen in solution[42]. From the polarization curve in Fig. 6 and the data in Table 2, it was also identified that the Tafel beta slope (β_c) changed with increasing temperature. Under conditions with the addition of TCF, it tended to be smaller (less

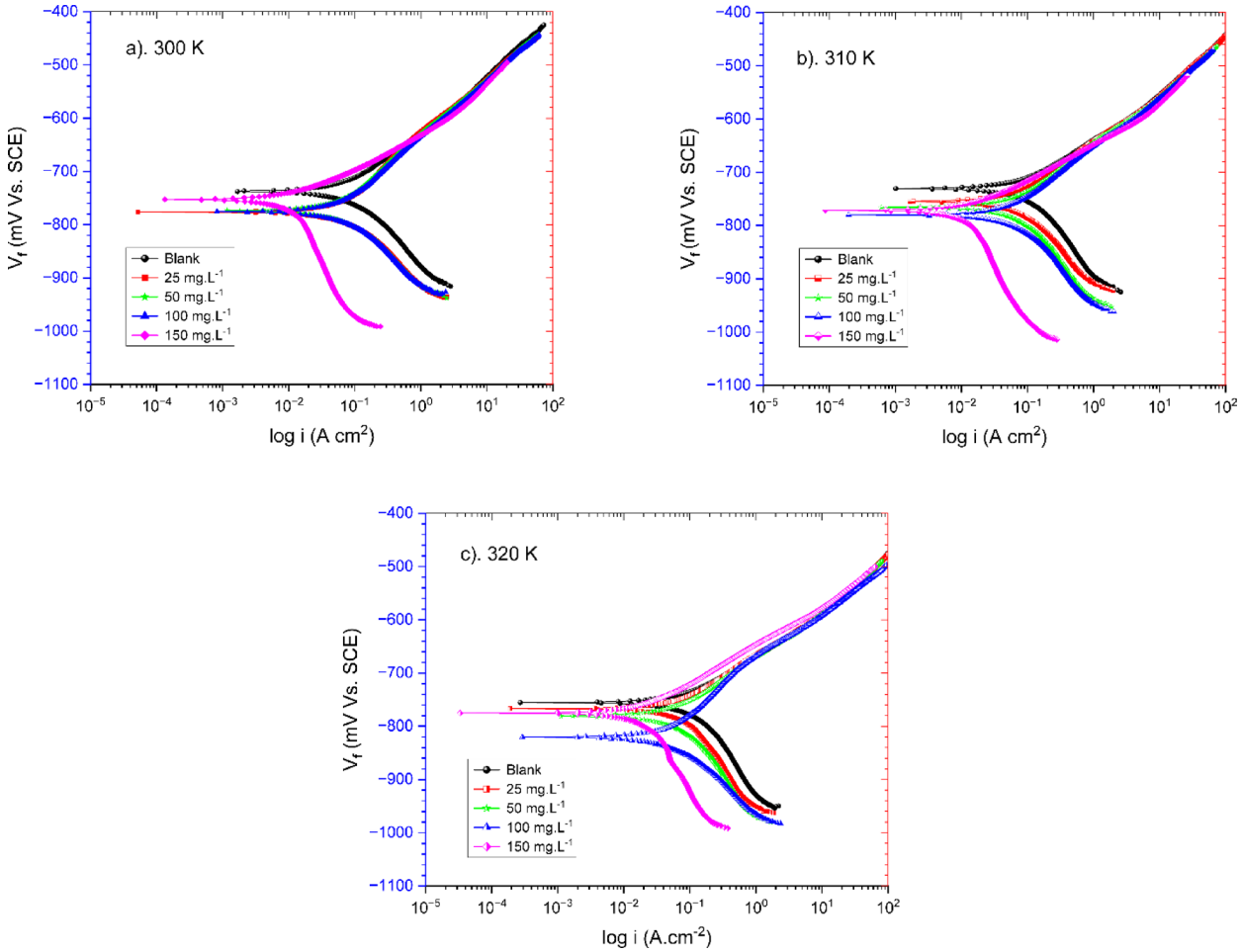

Fig. 6. Potentiodynamic polarization (PDP) curves of carbon steel in seawater with the absence and presence of varying TCF at (**a**) 300 K, (**b**) 310 K, and (**c**) 320 K.

T (K)	Con. (mg.L^{-1})	$-\beta_c$ (mV.dec^{-1})	E_{corr} (mV)/$_{SCE}$	I_{corr} (µA.cm^{-2})	*CR* (mmpy)	*IE* (%)
300	0	195.60	737.70	102.70	1.192	0.00
	25	108.60	776.40	62.69	0.728	38.94
	50	125.60	773.30	38.02	0.441	62.98
	100	193.90	775.40	34.67	0.403	66.23
	150	177.40	752.50	9.36	0.109	90.89
310	0	166.80	730.40	104.90	1.218	0.00
	25	106.10	755.20	64.27	0.746	38.75
	50	110.30	765.60	43.37	0.503	58.67
	100	151.50	780.00	40.58	0.471	61.33
	150	161.70	771.40	13.19	0.153	87.43
320	0	141.10	755.40	113.80	1.321	0.00
	25	87.32	766.80	71.94	0.835	36.78
	50	91.98	871.00	51.95	0.603	54.33
	100	113.60	820.10	48.49	0.563	57.39
	150	127.80	774.90	18.50	0.215	83.74

Table 2. Potentiodynamic electrochemical parameters of carbon steel in seawater containing *TCF* at different temperatures.

sharp) than in the blank solution. This shift in the Tafel slope confirms that the TCF affects the corrosion process (cathode) across all temperature ranges, a characteristic of the inhibitor[44].

The PDP curve (Fig. 6) also shows a decrease in extensive corrosion current density (I_{corr}) with TCF. The reduction in corrosion current density (I_{corr}) and the negative change in corrosion potential (E_{corr}) indicate that TCF molecules are adsorbed onto the steel surface[45], thereby establishing a protective film[46]. This film effectively blocks the active sites, inhibiting the electrochemical reactions responsible for metal dissolution[46]. The inhibition efficiency is moderate at low concentrations of TCF (25 to 100 mg.L^{-1} TCF). The drop in corrosion current density (I_{corr}) is apparent under these conditions, implying that the inhibitor may function by adsorbing onto the steel surface and forming a protective layer. However, the effect is less pronounced than at higher concentrations (150 mg.L^{-1}). This result implies that < 100 mg.L^{-1} TCF can provide some protection but may not fully prevent corrosion in this condition. Furthermore, at higher concentrations (150 mg.L^{-1}), I_{corr} decreased significantly, indicating that the inhibitor provided stronger protection, with a clear decrease in the corrosion rate.

However, the corrosion current density (I_{corr}) increases with temperature due to the increasing rate of iron anode dissolution and hydrogen ion cathode reduction (H^+)[47]. At 300 K, I_{corr} shows a lower value with a stronger inhibitor effect. At 310 K, I_{corr} increases slightly, but the inhibitor effect is still visible. At 320 K, I_{corr} increases sharply, indicating that high temperatures reduce the effectiveness of the inhibitor and increase the corrosion rate. In conditions without an inhibitor, I_{corr} is approximately 102.70 µA/cm^2 at 300 K and increases to 113.80 µA/cm^2 at 320 K. This increase in corrosion current indicates that temperature accelerates the corrosion process. As a result, the corrosion rate increases significantly at high temperatures. Under conditions with TCF (150 mg.L^{-1}), I_{corr} was 9.36 µA.cm^{-2} at 300 K and increased to 18.50 µA.cm^{-2} at 320 K. Although there was still an increase in I_{corr} with temperature, the increase was significantly smaller than that of the I_{corr} in the blank specimen, reflecting the inhibitor's ability to reduce the corrosion rate. This case demonstrates that the TCF inhibitor effectively inhibits the corrosion process, even at high temperatures, although its effectiveness (*IE*) decreases slightly with increasing temperature.

The inhibition efficiency of TCF was determined using the approach described by Eq. (1), which resulted in inhibition efficiency (%IE) values increasing with increasing TCF concentration. The increase in inhibition efficiency with TCF concentration up to a certain point is consistent with the typical behaviour of corrosion inhibitors. A relatively low *IE* was generated at low concentrations (below 100 mg.L^{-1}), possibly due to insufficient adsorption to completely cover the metal surface, leading to a lower inhibition rate (66.23% for 100 mg.L^{-1}). As the concentration increased (150 mg.L^{-1}), more inhibitor molecules were available to adsorb on the steel surface, leading to a higher inhibition efficiency (about 90.89%) at 300 K. At this concentration of TCF, the inhibition efficiency reached its highest value, indicating that this concentration is optimal for reducing the corrosion rate of carbon steel in seawater media well.

Potentiodynamic polarisation data measurements (Table 2) confirmed that TCF acted as an effective corrosion inhibitor for carbon steel in a seawater medium. The declining trend in the corrosion current density at higher concentrations indicated that TCF could be preferentially adsorbed to the active regions on the steel surface, thereby creating a barrier to corrosive species[48]. The inhibition efficiency of TCF observed in this study is comparable to that of other organic inhibitors, such as rice straw extract (92%) in a NaCl solution[49]. Additionally, this result aligns with previous studies on the effect of inhibitor concentration on seawater media, where efficiency increases with increasing concentration[50]. These efficiency results emphasize the promise of TCF as a corrosion inhibitor, although further investigation is recommended to explore its long-term stability and effectiveness in real-world applications.

Electrochemical impedance spectroscopy (EIS) analysis

Figure 7 displays the effects of different TCF concentrations (blank, 25 mg.L^{-1} to 15 mg.L^{-1}) on the performance of carbon steel using an electrochemical technique in a seawater medium. The electrochemical parameter data from fitting using a circuit model (in Fig. 8) were tabulated in Table 3.

As shown in Figs. 7a, b, c, the Nyquist plot results display a semicircular curve associated with charge transfer resistance (R_{ct}) and double-layer capacitance (C_{dl}). According to the Nyquist plot, the diameter of the semicircle increases as TCF concentration increases. This results in a rise of charge transfer resistance (R_{ct}), which implies a reduction in corrosion rate[11]. The addition of TCF enhances the formation of a protective layer on the carbon steel surface, thereby protecting against the electrochemical reactions that cause corrosion[51]. At the lowest concentration of TCF (25 mg.L^{-1}), the resulting R_{ct} is relatively low, indicating limited protection. The increase in corrosion resistance occurs at concentrations of 100 mg.L^{-1} and 150 mg.L^{-1}, suggesting that forming a perfect passive layer more effectively inhibits corrosion[52]. Higher R_{ct} values indicate more efficient corrosion inhibition, as the TCF molecules interact with the steel surface, reducing the active area accessible for corrosive attack[51]. Furthermore, increasing temperature causes a decrease in R_{ct}, indicating that the temperature effect can reduce the inhibitor's ability to form an effective passive layer[53].

The Bode plot results (Figs. 7a', b', c') confirm the stability of the protective layer, where at a concentration of 25 mg.L^{-1}, it shows a lower impedance at low frequencies, indicating a less stable passive layer. At concentrations of 100 mg.L^{-1} and 150 mg.L^{-1}, it exhibits a very high impedance, indicating the formation of a stable and effective protective layer. This result is also reinforced by the phase angle value, which increases with the addition of inhibitors, indicating that the capacitive properties of the protective layer become increasingly stable and uniform[54]. The Bode plot and phase angle show a decrease with increasing temperature, indicating a reduction in the stability of the protective layer[51]. The Nyquist and Bode plots in this study suggest that TCF is an effective inhibitor of carbon steel in seawater. The increments in charge transfer resistance (R_{ct}) and the improvement in phase angle (θ) at higher TCF concentrations indicate the potential to establish a stable, protective barrier on the steel surface. These electrochemical results are consistent with the previous study[46], which has demonstrated the

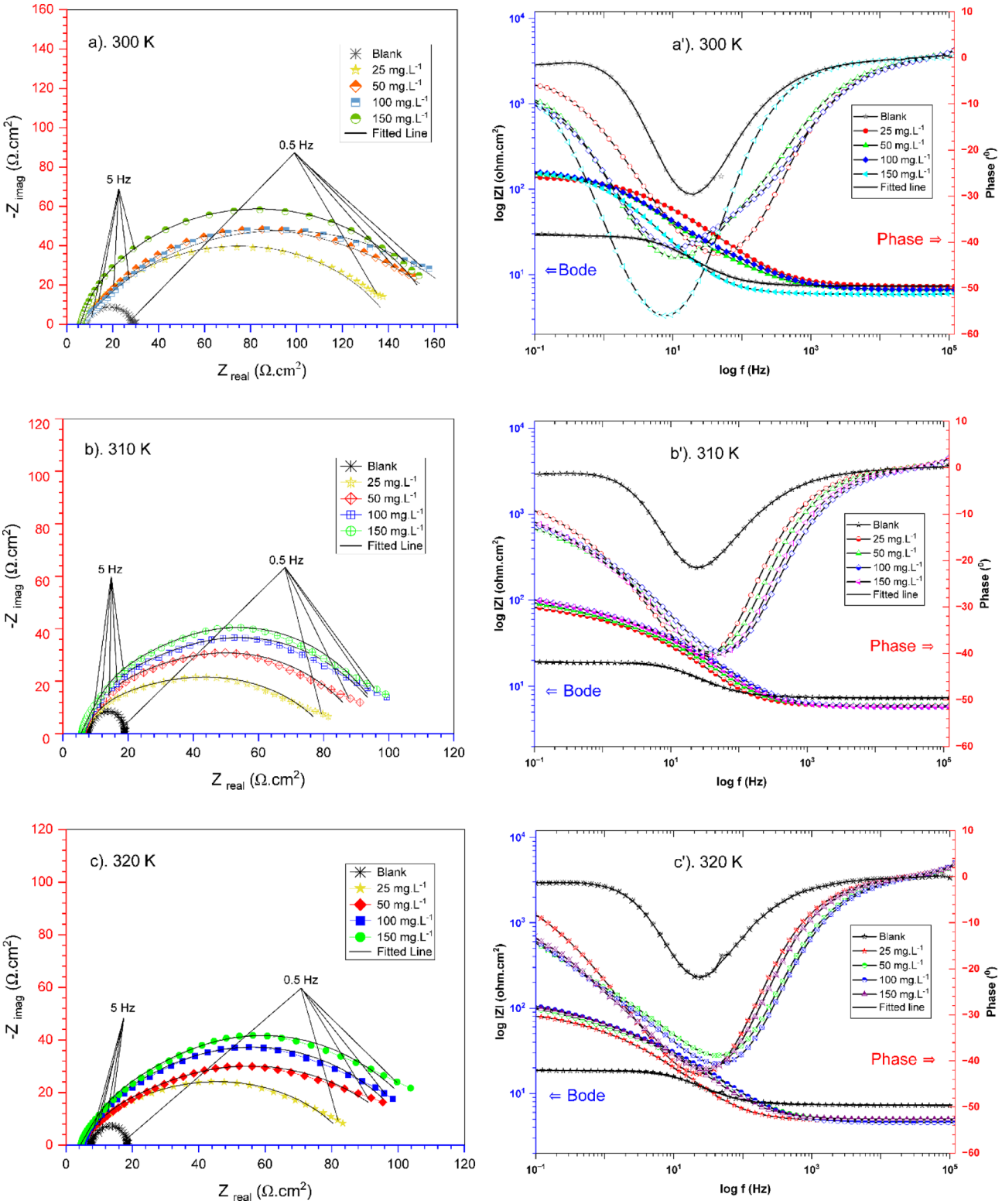

Fig. 7. Nyquist and Bode plots of carbon steel in seawater with the absence and presence of varying TCF at (**a** and **a'**) 300 K, (**b** and **b'**) 310 K, and (**c** and **c'**) 320 K.

effectiveness of ascorbic acid as a green corrosion inhibitor for API 5L ×60 by adsorption on the metal surface and creating a protective barrier against aggressive ions in seawater environments.

Table 3 summarises the EIS parameter data by matching the spectrum data to the corresponding electrical model illustrated in Fig. 8, which provides a better understanding of the electrochemical behaviour. The components of this electrical circuit include electrolyte resistance (R_e), charge transfer resistance (R_{ct}), film

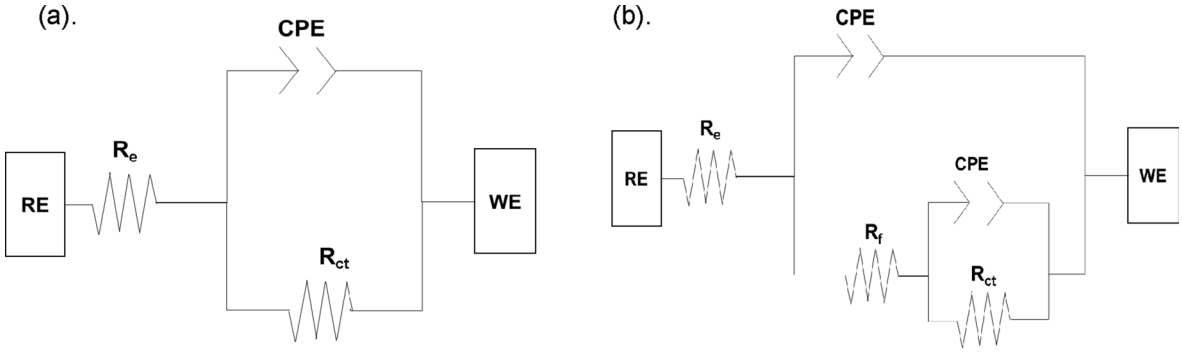

Fig. 8. The circuit model used in interpreting TCF performance analysis is (**a**) blank and (**b**) with TCF.

T (K)	Con. (mg.L^{-1})	R_e (Ω.cm^2)	R_{ct} (Ω.cm^2)	R_f (Ω.cm^2)	$R_p = R_{ct} + R_f$ (Ω.cm^2)	C_{dl} (μF.cm^{-2})	Y_o ($10^{-6} \times \Omega^{-1}$ cm^{-2} S^n)	n	η (%)
300	0	7.35	21.80	0.00	21.80	707.1	1288	0.87	0.00
	25	7.14	32.50	2.03	34.53	786.0	1649	0.70	36.87
	50	6.56	37.60	3.40	41.00	381.2	1590	0.66	46.83
	100	6.52	54.30	4.25	58.55	344.4	1535	0.64	62.77
	150	5.92	275.20	6.02	281.22	169.0	863.7	0.83	92.25
310	0	7.37	11.90	0.00	11.90	747.2	1477	0.86	0.00
	25	5.75	15.51	1.74	17.25	429.0	2344	0.69	31.01
	50	5.70	18.47	1.40	19.87	351.2	2180	0.65	40.11
	100	5.52	25.75	3.34	29.09	297.6	2046	0.63	59.09
	150	5.51	115.50	5.23	120.73	249.0	2025	0.65	90.14
320	0	7.33	11.39	0.00	11.39	850.5	1527	0.88	0.00
	25	4.67	12.29	1.34	13.63	562.8	3043	0.70	16.43
	50	4.53	15.82	1.98	17.80	492.2	2702	0.61	36.01
	100	4.80	19.70	2.39	22.09	393.0	2646	0.66	48.44
	150	4.32	106.10	4.40	110.50	372.0	2399	0.62	89.69

Table 3. Electrochemical parameters for carbon steel in seawater with different temperatures and TCF concentrations.

resistance (R_f), and a constant phase element (*CPE*). Because an inhomogeneous steel surface is considered, the double-layer capacitance (C_{dl}) was replaced by the constant phase element (*CPE*) to provide a more accurate matching[38]. The *CPE* impedance function is represented in the following Eq. 11 [55]:

$$Z_{CPE} = Y_0^{-1}(i\omega)^{-n} \tag{11}$$

In this case, the notation of i, ω, Y_0, and n represents the imaginary unit ($i^2 = -1$), angular frequency ($\omega = 2\pi f$), the *CPE* constant, and the *CPE* exponent, respectively, with values spanning from −1 to 1. Additionally, the subsequent formula (Eq. 12) establishes a relationship between the *CPE* and C_{dl}[56]:

$$C_{\mathrm{dl}} = \sqrt[n]{Y_0 . R_P^{1-n}} \tag{12}$$

The data in Table 3 reveal that the electrolyte resistance (R_e) tends to decrease at higher temperatures. At higher temperatures, the molecules in the solution become more active, which can increase the corrosion rate[41]. This increase is attributed to the acceleration of the oxidation process in the metal, resulting in a decrease in electrolyte resistance (R_e)[29]. At higher temperatures, although the inhibitor still functions, the increase in the corrosion rate can reduce the effectiveness of the inhibitor protection, leading to a decrease in resistance. The decreasing trend of n values with the concentration amount is due to the increasing non-uniformity of the substrate produced by the active molecules adsorbed on the steel surface[57,58]. The rising trend of R_{ct} values with increasing concentrations of TCF indicates that the active molecules of TCF are adsorbed on the carbon steel surface exposed to seawater media, blocking the active areas exposed to corrosive agents and producing a thin protective layer at the metal-solution interface.

The results showed that temperature has a substantial impact on the corrosion reaction of carbon steel in seawater media. In the absence of TCF, the corrosion rate increased significantly with temperature, as expected, due to the improved reaction kinetics[51]. The addition of TCF reduced this temperature-dependent corrosion

acceleration, making the effect more significant as the inhibitor concentration increased. With 150 mg.L^{-1} of TCF, the inhibition efficiency was high throughout the temperature range, although it decreased slightly with increasing temperature. At 300 K, the efficiency (%η) was about 92.25%, while at 310 K, the efficiency (%η) decreased to about 90.14%. This decrease is likely due to the reduced efficiency of inhibitor adsorption at higher temperatures[59,60], which can weaken the protective layer. However, at 320 K, despite the decreased efficiency, the inhibitor still provided significant protection, reducing the corrosion rate by about 89.69% compared to the blank specimen. The decrease in inhibition efficiency at high temperatures is due to the decreased adsorption strength of the TCF on the steel surface. At high temperatures, the molecular reaction process between the steel surface and the inhibitor becomes weaker[61,62], which causes a decrease in the effectiveness of the protective layer.

Thermodynamic and adsorption studies

To fully understand the effectiveness of TCF as a corrosion inhibitor, it is important to investigate its behavior through thermodynamic, kinetic, and adsorption analysis. These analyses help determine the inhibition mechanism, activation energy, adsorption characteristics, and the correlation between temperature and inhibitor concentration. Increasing temperature can significantly influence the characteristics of steel materials, including kinetics, corrosion rate, and equilibrium. The Arrhenius equation, expressed in Eq. (13) [63], can be applied to investigate the relationship between corrosion rate and temperature factors.

$$\log \mathrm{CR} = \frac{-E_a}{2.303R}\left(\frac{1}{T}\right) + \log A \tag{13}$$

$$\log \frac{CR}{T} = \left(\log \frac{R}{N_A h} + \frac{\Delta S_a}{2.303R}\right) - \left(\frac{\Delta H_a}{2.303R}\frac{1}{T}\right) \tag{14}$$

The notation E_a, A, R, ΔH_a, ΔS_a, h, N_A, *and* T represent the activation energy, the Arrhenius factor, the gas constant, the activation enthalpy, the activation entropy, the Planck constant, the Avogadro number, and the temperature in kelvin, respectively. Figure 9a shows how the slop of the log (CR) = f (10^3 T^{-1}) curve was applied to determine E_a. Table 4 lists the values of the Arrhenius factor (A), ΔS_a, and ΔH_a, which were obtained from both the intercept and the slope of the log (CR/T) = f (10^3 T^{-1}) curve (Fig. 9b) followed in Eq. (14) [64].

The corrosion current density (I_{corr}) exhibits an Arrhenius-type behaviour with temperature, indicating that the corrosion rate increases with rising temperature. The activation energy (E_a) for corrosion can be determined by plotting ln (I_{corr}) vs. 1/T. For the blank solution, the activation energy (E_a) obtained was 4.07 kJ mol^{-1} (lower than the condition with the addition of TCF), indicating that the corrosion mechanism is thermodynamically favourable and easy to initiate. The increase in E_a (5.45 to 27.22 kJ.mol^{-1}) suggests that the inhibitor effectively blocks the corrosion reaction[65], which requires more energy to initiate the electrochemical reaction. This behaviour is typical of inhibitors adsorbed on the metal surface, slowing down the corrosion reactions[66]. Several studies have shown that E_a for the blank solution tends to decrease with increasing temperature, indicating that corrosion becomes easier to initiate at higher temperatures[29]. On the contrary, the activation energy slightly increases with the presence of an inhibitor, indicating that the inhibitor reduces the thermodynamic properties of corrosion and makes it difficult for the electrochemical reaction to occur, even at higher temperatures[27]. The positive value of ΔH illustrates the endothermic process in the reaction[67].

Thermodynamic parameters of corrosion inhibition, such as adsorption-free energy (ΔG_{ads}), are essential to understanding the effectiveness of inhibitors. The Langmuir adsorption isotherm was employed to assess the adsorption of TCF onto steel surfaces. Langmuir isotherm interprets that the adsorption sites on the steel surface

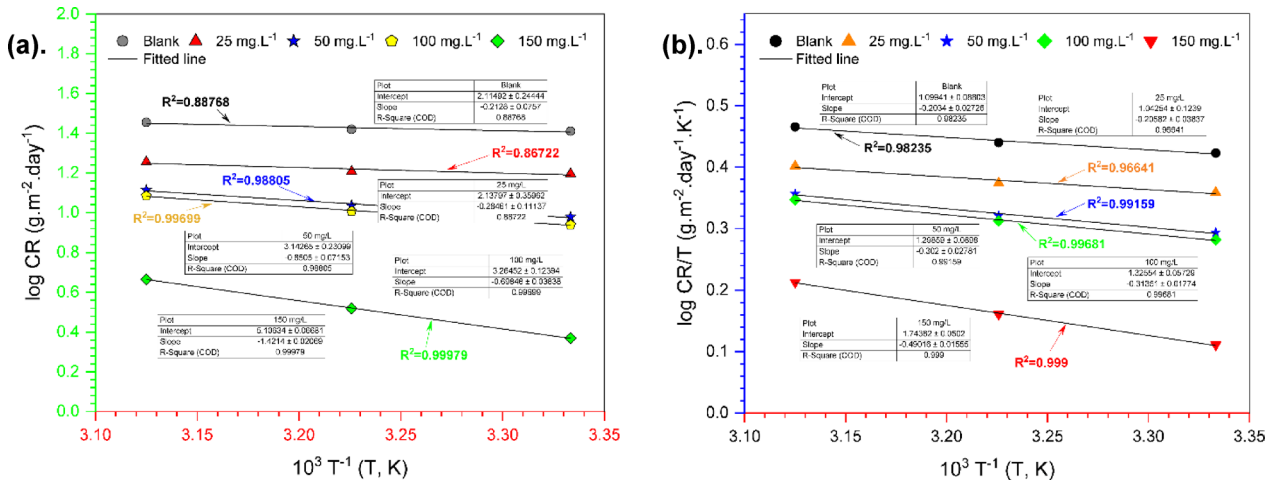

Fig. 9. Arrhenius plots (**a**) and Arrhenius transition plots (**b**) for carbon steel in seawater medium in the absence and presence of the inhibitor TCF.

Condition	E_a (kJ.mol^{-1})	A (g.m^{-2}.min^{-1})	ΔH_a (kJ.mol^{-1})	ΔS_a (J.mol^{-1}.K^{-1})
Blank	4.07	130.29	3.89	− 101.96
25 mg.L^{-1}	5.45	137.40	3.94	− 102.02
50 mg.L^{-1}	12.46	1388.67	5.78	− 101.76
100 mg.L^{-1}	13.37	1838.65	6.00	− 101.74
150 mg.L^{-1}	27.22	127,732.08	9.39	− 101.32

Table 4. Thermodynamic activation parameters for carbon steel resulted in the absence and presence of various TCF concentrations.

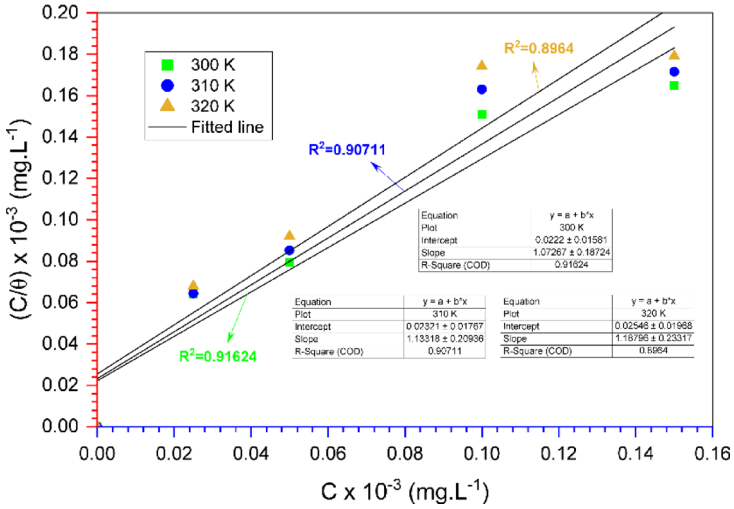

Fig. 10. Langmuir adsorption isotherm of TCF on carbon steel in seawater medium.

Conditions	K_{ads} / (mg. L^{-1})	R^2	ΔG_{ads} (kJ.mol^{-1})
300 K	4.50×10^{-2}	0.91624	− 26.73
310 K	4.31×10^{-2}	0.90711	− 27.51
320 K	3.93×10^{-2}	0.89640	− 28.15

Table 5. Adsorption parameters for the concentration effect of carbon steel in seawater medium at 300 K, 310 K, and 320 K.

are equivalent and that the adsorption of inhibitor molecules occurs independently, without interaction between the adsorbed molecules. The adsorption isotherm can be formulated as follows in Eq. (15) [68]:

$$\frac{C}{\theta} = \frac{1}{K} + C \tag{15}$$

where θ denotes the surface fraction covered by the inhibitor (IE/100), C represents the inhibitor concentration, and K_{ads} is the adsorption equilibrium constant.

From the Langmuir plot (C/θ vs. C) as displayed in Fig. 10, a linear relationship can be obtained, and the slope of the line represents $1/K_{ads}$, which allows the determination of the adsorption constant. The higher the K_{ads}, the stronger the correlation between the steel surface and the inhibitor, indicating a better inhibition effectiveness.

Furthermore, the standard adsorption free energy (ΔG_{ads}) is the main parameter that could be calculated from the adsorption equilibrium constant (K_{ads}) using the following Eq. (16) [51]:

$$\Delta G_{ads} = -2.303RT \log\left(10^6 \cdot K_{ads}\right) \tag{16}$$

In this adsorption case in the corrosion field, R and 10^6 denote the gas constant and H_2O concentration, respectively. Table 5 depicts the adsorption parameters of TCF on carbon steel surfaces in seawater. In conditions without an inhibitor (blank), there is no adsorption process; therefore, ΔG_{ads} is not valid (not determined). In the presence of TCF, ΔG_{ads} is obtained around − 26.73 kJ.mol^{-1} to − 28.15 kJ.mol^{-1}, a negative value characteristic of the spontaneous adsorption[5]. Various literatures show that chemisorption occurs when the ΔG value is less than

– 40 kJ/mol. The combined physisorption-chemisorption process, or mixed type, occurs when the ΔG value is between – 40 and – 20 kJ.mol^{-1}. Furthermore, physisorption occurs when the ΔG value exceeds – 20 kJ/mol. In this work, the ΔGa_{ds} value, ranging from – 26.73 kJ/mol to – 28.15 kJ/mol, indicates that the inhibitor exhibits a mixed type of physisorption-chemisorption adsorption onto the steel surface[69], resulting in a correlation between the carbon steel surface and the inhibitor.

The inhibition mechanism of TCF is likely to inhibit corrosion through physical and chemical adsorption mechanisms, forming a protective barrier on the steel surface. The efficiency of the inhibitor rises with concentration, although its effectiveness decreases with increasing temperature. The ability of the inhibitor to decline the anodic dissolution process ($Fe \rightarrow Fe^{2+}$) and cathodic hydrogen evolution ($2H^{+} + 2e^{-} \rightarrow H_2$) indicates a mixed-type inhibition mechanism. At lower concentrations, TCF is predicted to be adsorbed to the steel surface through van der Waals forces or electrostatic interactions, forming a protective film that prevents direct contact between the metal surface and the corrosive medium. The effectiveness of physical adsorption is temperature dependent, with higher temperatures potentially weakening the adsorption bond[70]. At higher concentrations or temperatures, TCF can form stronger bonds with the steel surface, indicating chemisorption[69]. The presence of nitrogen and amines in the TCF structure can facilitate the formation of coordinate bonds with the steel surface, thereby enhancing the protective effect of the inhibitor.

Comparison, potential application, and future studies

Detailed comparisons with other natural extracts, insights into applications, and suggestions for future studies are crucial for highlighting the significance of the findings and exploring their broader implications. Numerous studies have investigated the use of natural plant extracts as corrosion inhibitors for carbon steel. For example, *Carob fruit, Bidens pilosa, Manihot esculenta, Catharanthus roseus,* and *Tinospora crispa* have been well documented. These studies reported corrosion inhibition efficiencies in the 60–90% range in almost the same media, namely sodium chloride or seawater environments, as tabulated in Table 6. In terms of inhibition efficiency, the efficiency in this study is more competitive than that of several previous studies, where remarkable corrosion inhibition efficiencies were achieved (90.89% with PDP and 92.25% with EIS) at a relatively low dose (150 mg.L^{-1}). These higher efficiency results are possible because the active compounds are purer than in previous studies[27], where the extracts were initially fractionated, allowing the role of the active substances to be more optimal than that of the crude extract. However, some natural extracts, such as *Nigella sativa L.* and *Apple pomace*, showed slightly higher efficiencies, with 94% and 98.8% efficiency values, respectively[9,71]. The increase in inhibition efficiency can be attributed to the increased concentration applied and decreases with increasing temperature[40,41]. Different inhibition efficiencies are also influenced by the various types of extract solvents used because they produce different bioactive compounds[72].

Furthermore, the presence of functional groups such as –OH, –NH_2, –C=O, and aromatic rings can enhance adsorption on metal surfaces by donating electrons or forming coordinate bonds with the metal surface[73]. In addition to the preparation of extracts and the concentration of inhibitors, the type and concentration of corrosive species, such as chloride (Cl^-) and sulfate (SO_4^{2-}), as well as aggressive ions, also influence the effectiveness of inhibitors because they can form complexes with corrosive ions, thereby reducing their effectiveness[74]. Furthermore, electron-donating capacity (HOMO–LUMO gap) and polarizability also contribute to differences in inhibition ability. Therefore, quantum chemical computations are crucial for predicting and rationalizing inhibition performance.

Years	Green inhibitor	Solvent	Metal (medium)	Concentrations	IE (%)	Ref
2025	TCF	Methanol–water	Carbon steel (seawater)	150 mg.L^{-1}	90.89 (PDP) & 92.25 (EIS)	In this work
2024	*Trifolium repens*	Dichloromethane	API 5LX60 (3.5% NaCl)	20 ppm	98	40
2024	*Nigella sativa L*	Water	Mild steel (3.5% NaCl)	600 ppm	94.00	9
2024	*Bidens pilosa*	Ethanolic exxtract	Carbon steel SAE 1008 (0.1 M NaCl)	1000 ppm	83.00	75
2024	Carob fruit extract (CFE)	70% methanol	Cu-Ni alloys (3.5% NaCl)	300 ppm	92.60	42
2024	Dandelion root	Ethanol	Steel, TH-550 & TS-275 (3% NaCl)	1.5 g.L^{-1}	85.35 (TH) & 79.98 (TS)	76
2024	*Cashew leaf + AgNPs*	Ethanol	Mild steel (3.5% NaCl)	0.3 g.L^{-1}	94.3	77
2023	T. cordifolia	Methanol–water	Mild steel (artificial seawater)	300 ppm	85.94	27
2023	Manihot esculenta	Buffer	AISI 1015 (3.5% NaCl)	20 mg.L^{-1}	88.37	43
2023	*Artemisia annua L*	Artificial seawater	Aluminium alloy (artificial seawater)	1 g.L^{-1}	66.7	78
2022	*Ceriops tagal*	Salt	Steel Q235 (3.5% NaCl)	3 g.L-1	60.51	36
2021	*Peach pomace*	Mix of propanol/ethanol/water	Mild steel (0.5 M NaCl)	800 ppm	94.2	79
2020	Catharanthus roseus	Ethanol	Mild steel (3.5% NaCl)	5 mg.L-1	74	80
2020	*Apple pomace*	Urea	Steel C1010 (3.5% NaCl)	3%	98.8	71
2019	*Persian liquorice*	–	Mild steel (3.5% NaCl)	600 ppm	98.8	81
2019	*Juglans regia*	Water	Mild steel (3.5% NaCl)	1000 ppm	94	55
2018	*Combination of green organic*	NaCl	Mild steel (3.5% NaCl)	3%	89	82
2016	*Tinospora crispa*	Distilled water	Mild steel (1 mol.L^{-1} HCl)	800 ppm	78.14	26

Table 6. Comparative efficiency of TCF with several previous studies.

The potential utilization of *Tinospora cordifolia* extract from this study presents a more environmentally friendly and sustainable alternative to traditional synthetic inhibitors, which may be toxic or harmful to the environment. The practical application of TCF can be applied to structures in contact with seawater where corrosion resistance in saline environments is critical. In addition, TCF can be incorporated into coatings or surface treatments to enhance the corrosion resistance of metals exposed to seawater. Future developments should optimize the extraction method to maximize the concentration of active compounds in *Tinospora cordifolia*, which are responsible for corrosion inhibition. Standardization of the extract formulation for large-scale applications may make it more feasible for industrial use. Furthermore, long-term studies are necessary to evaluate the durability of its protective effects, particularly under fluctuating seawater conditions and varying temperatures.

Surface morphology studies

SEM–EDX analysis

The effectiveness of TCF as a green corrosion inhibitor for carbon steel in seawater medium can be further explained through morphological and surface analysis. Understanding the surface characteristics of carbon steel before and after exposure to inhibitors provides insight into the protection mechanism and effectiveness of bioactive compounds. Figure 11 illustrates the morphological examination of polished carbon steel surfaces before and after being soaked in seawater with the absence and presence of 150 $mg.L^{-1}$ TCF for 24 h. The carbon steel surface (Fig. 11a) appears well-polished, smooth, and free of spots.

SEM morphology (Fig. 11b) of carbon steel exposed to seawater media without inhibitors shows significant corrosion features, including peeling, surface roughness, and formation of corrosion products. Corrosion sites indicate an aggressive attack, such as the presence of chloride ions, which cause rapid metal dissolution[83]. In contrast, SEM images of carbon steel exposed to TCF show a smoother surface with fewer corrosion features. The protective layer formed by the adsorption of bioactive compounds appears to inhibit the penetration of corrosive agents, thereby reducing peeling and surface degradation[38]. This result suggests that the inhibitor effectively protects mild steel from corrosion. Similar results were found on the surface of AISI 1015 steel substrates exposed to 3.5% NaCl media, where the metal substrate surface displayed severe corrosion in the absence of the green inhibitor (Cassava leaf), and the corrosion decreased significantly with the addition of the inhibitor[43]. Furthermore, elemental EDX results of the steel surface also show the distribution of elements such as iron, oxygen, and elements associated with *Tinospora cordifolia* extracts (e.g., carbon from organic compounds). The presence of carbon on the surface after treatment with inhibitors indicates successful adsorption of plant compounds[76].

AFM analysis

Furthermore, AFM provided high-resolution surface topography images, enabling the assessment of surface roughness and texture. From the AFM results (Fig. 12), the carbon steel sample's average surface roughness (Ra) value after being added to TCF was much lower than that of the carbon steel after exposure without TCF. The significant reduction in Ra with inhibitors indicates that the surface becomes smoother due to the formation of a protective layer[9]. The AFM image also shows a homogeneous distribution of the protective layer, confirming the adsorption of active substance molecules from TCF onto the steel surface. The ability of bioactive compounds to cover the surface evenly increases corrosion resistance[40].

UV–Vis analysis

The process of inhibiting steel corrosion in corrosive media with green inhibitors is typically associated with the absorption of active compounds from the extract onto the steel surface. To demonstrate absorption, a UV–Vis test was conducted on the TCF solution before and after exposure, and the results are presented in Fig. 13. The UV–Vis spectrum of TCF before exposure to carbon steel in seawater will show a clear absorption peak (green line), indicating the presence of certain phytochemical compounds, such as alkaloids, tannins, flavonoids, phenolics, or flavonoids, as in section "UV–Vis characteristics". These compounds have the potential to inhibit corrosion by forming a protective layer on the metal surface. The UV–Vis spectrum shows significant changes after exposure to carbon steel in seawater media (red line). In the spectrum after exposure, there is a shift in the absorption peak (308 nm to 298 nm, Tannin), a reduction in peak intensity for alkaloids, and the disappearance of peaks (phenolics and flavonoids), which will indicate that interactions have occurred between compounds from TCF and the metal surface. The decrease and disappearance of the spectrum in the UV–Vis results of the solution after exposure can be correlated with the corrosion rate data obtained from electrochemical measurements (PDP and EIS), where the inhibition efficiency increases, indicating that phytochemicals play an active role in corrosion inhibition by adsorbing to the metal surface and forming a protective barrier.

XPS analysis

Furthermore, to confirm the chemical composition and state of the elements on the carbon steel surface, an evaluation was conducted using X-ray photoelectron spectroscopy (XPS), with the results presented in Fig. 14. Figure 14 illustrates the XPS survey scan and deconvoluted peaks of each spectrum for the carbon steel surface (blank), exposed steel without and with 150 $mg.L^{-1}$ TCF. The binding energy values were corrected using the Kratos standard for the signal C1s atom (284.6 eV). The binding energy was calculated using a Shirley-type background and a Gaussian curve. Through the analysis of the electron binding energy in carbon (C 1s), oxygen (O 1s), iron (Fe 2p), and chloride (Cl 2p), valuable data can be obtained, as presented in Table 7. The Na 1 s and Cl 2p peaks were identified on the carbon steel specimen immersed in the solution, indicating that the solution used was rich in Na and Cl elements (seawater).

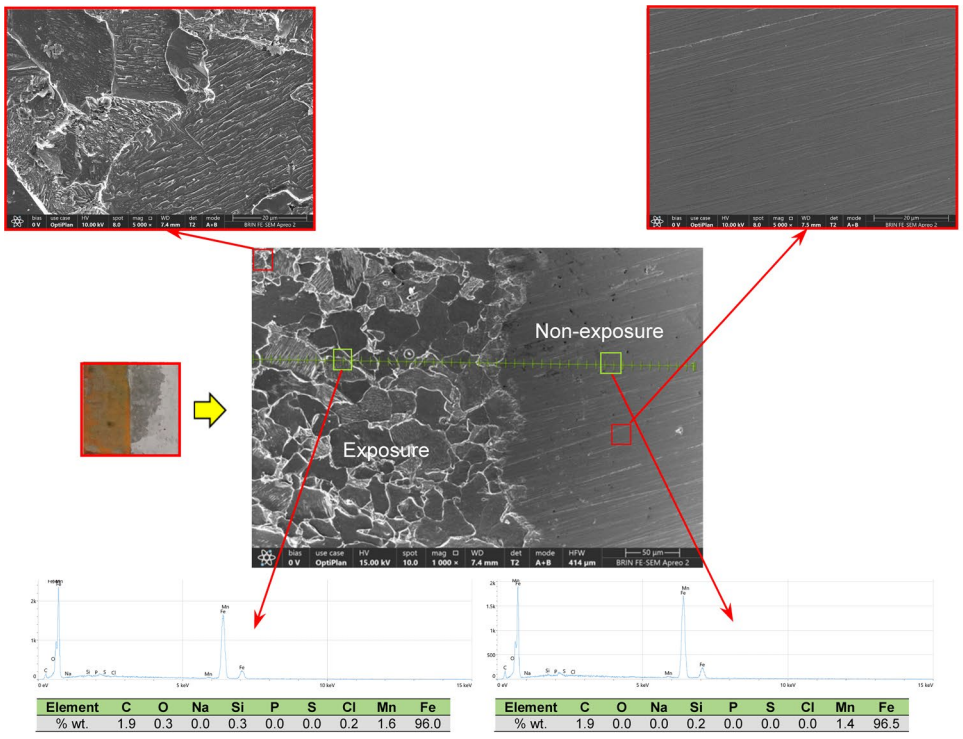

Element	C	O	Na	Si	P	S	Cl	Mn	Fe
% wt.	1.9	0.3	0.0	0.3	0.0	0.0	0.2	1.6	96.0

Element	C	O	Na	Si	P	S	Cl	Mn	Fe
% wt.	1.9	0.0	0.0	0.2	0.0	0.0	0.0	1.4	96.5

(a) FE-SEM and EDX of the carbon steel surface without TCF.

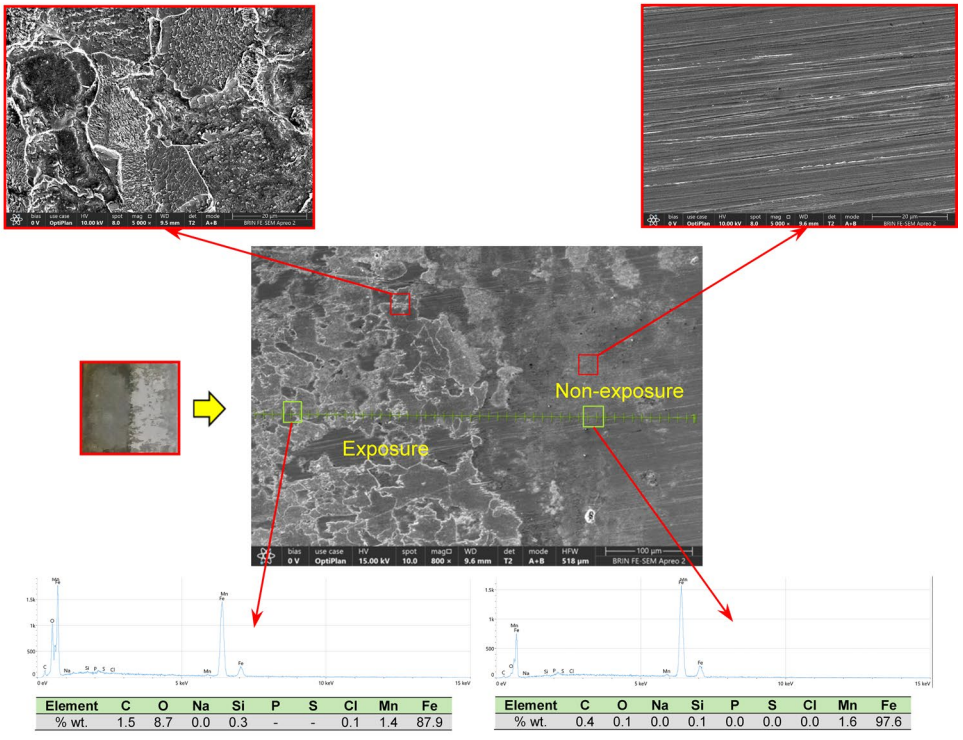

Element	C	O	Na	Si	P	S	Cl	Mn	Fe
% wt.	1.5	8.7	0.0	0.3	-	-	0.1	1.4	87.9

Element	C	O	Na	Si	P	S	Cl	Mn	Fe
% wt.	0.4	0.1	0.0	0.1	0.0	0.0	0.0	1.6	97.6

(b) FE-SEM and EDX of the steel surface with TCF.

Fig. 11. FE-SEM and EDX of the steel surface for (**a**) without and (**b**) with TCF.

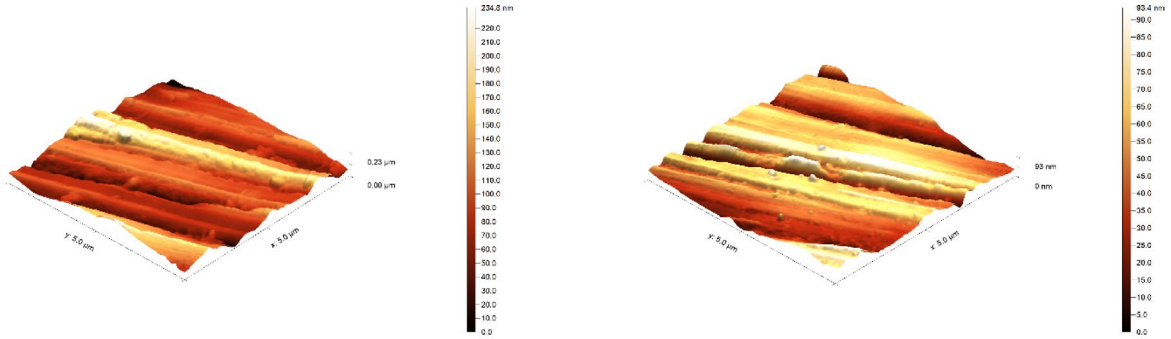

(a) With *T. cordifolia* fractions. (b) Without *T. cordifolia* fractions.

Fig. 12. AFM images of the steel surface for (**a**) with and (**b**) without TCF.

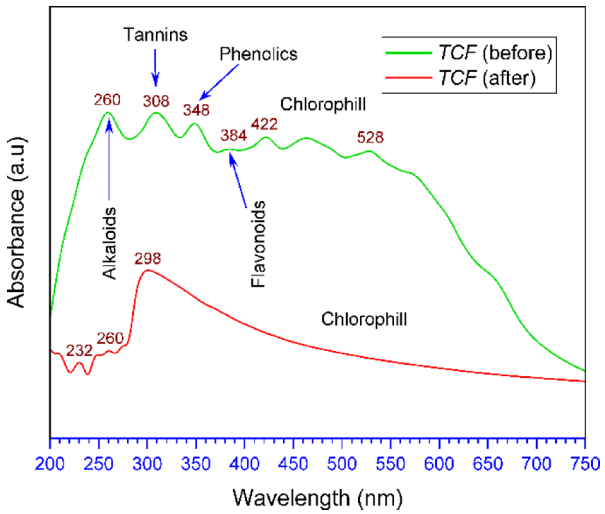

Fig. 13. UV–Vis spectra of TCF before and after exposure to carbon steel in seawater medium.

The C 1 s profile (non-TCF and TCF) showed several peaks at 284.61, 287.56, and 291.95 eV may be labeled as C–C, C=O, and C–O, while in the specimen with TCF at 284.61 eV may be attributed to C–C bonds, 285.58 eV can be recognized as C–O, or C–N bonds, and 288.79 eV can be attributed to N=C bond[84]. The Cl bands at the metal interface in specimens with and without TCF in seawater solution can be attributed to the attraction between Cl^- ions and the positive charge of the metal surface, resulting in the formation of iron(III) chloride[83]. The Cl 2p peak was detected at 197.46 eV and 198.96 eV for the non-TCF specimen and at 198.48 eV and 200.05 eV for the TCF specimen due to the presence of Cl 2p3/2[83]. The XPS profile of iron-2p was shown in the prominent peaks at around 710 eV and 724 eV, which were associated with Fe-2p3/2 of Fe(II)[85,86]. In addition, the O–1 s profile at peaks of 530 eV and 528 eV was suggested to be related to the O and OH–atoms bonded to Fe(II) and Fe(III) to form FeO/Fe2O3 and FeOOH oxides, respectively[87].

The shift in binding energy in the XPS spectrum can reveal changes in the oxidation state of iron and the formation of iron oxide or hydroxide species, indicating corrosion[10]. The presence of new peaks corresponding to functional groups from the TCF indicates that these compounds interact chemically with the steel surface, further increasing corrosion resistance[88].

The morphology and surface analysis results confirmed that TCF significantly enhanced the corrosion resistance of carbon steel in a simulated seawater medium. This finding was confirmed by the formation of a protective layer by bioactive compounds from TCF through the adsorption process to the steel surface, and a decrease in surface roughness and smoother surface morphology on the steel surface added with inhibitors, as well as the presence of chemical interactions between the inhibitor and the steel surface that can improve corrosion resistance.

Computation analysis

Experimental measurements have demonstrated that the bioactive compound in TCF (moupinamide) exhibits strong corrosion inhibition efficiency, with a protective efficacy exceeding 90% at a concentration of 150 $mg.L^{-1}$. To model and comprehensively understand the electronic properties of moupinamide and its interaction with

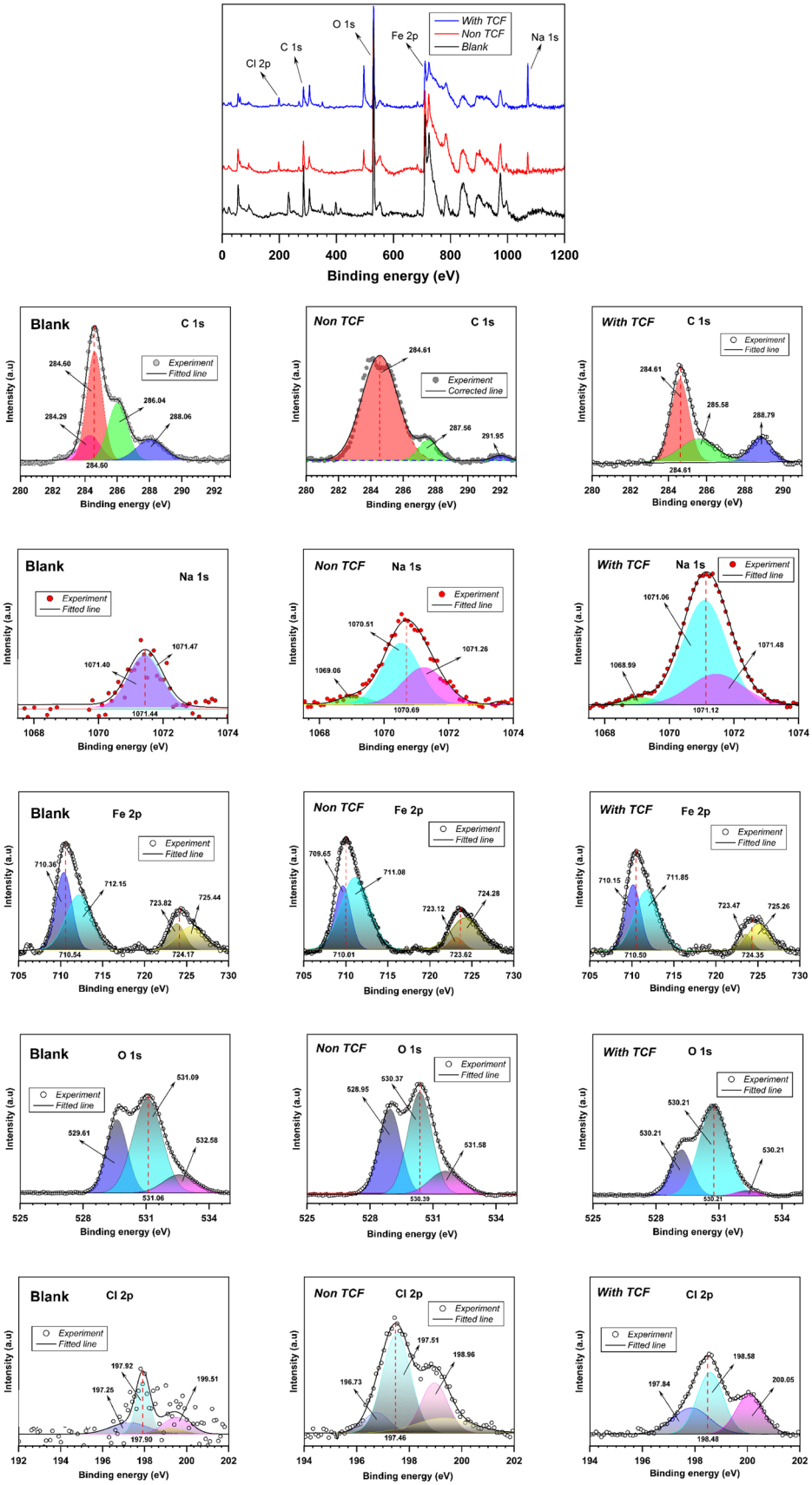

Fig. 14. XPS of carbon steel surface for: blank (left), without TCF (center), and with TCF (right).

Condition	Element											
	C 1 s		Na 1 s		Fe 2p		O 1 s		Cl 2p		N 1 s	
	BE	% mass	BE	% mass	BE	% mass	BE	% mass	BE	% mass	BE	% mass
Blank	284.70	16.7	1072.7	0.5	711.7	48.6	530.7	31.0	202.7	–	397.7	–
Non-TCF	284.67	13.1	1070.67	3.8	709.67	46.8	529.67	32.5	197.67	3.8	399.67	0.1
With TCF	284.6	13.2	1070.6	9.0	709.6	36.1	529.6	35.7	197.6	4.7	399.6	1.3

Table 7. Element composition and binding energy (BE) for blank, non-TFC, and with TCF of carbon steel by XPS survey.

the carbon steel surface, computations using density functional theory (DFT) were carried out. The results of the structure optimization, including the highest occupied molecular orbital (HOMO) and lowest unoccupied molecular orbital (LUMO), surface contour, total density, and electrostatic potential (ESP), are depicted in Fig. 15, along with detailed data of quantum chemical parameters tabulated in Table 8. HOMO describes the region that tends to donate electrons, while LUMO indicates the main electron-accepting region in a molecule[42]. As seen in Fig. 15, the electron distributions of HOMO and LUMO are primarily concentrated in the aromatic ring and N-trans double bond compounds, indicating their high ability in electron exchange and interaction with metal surfaces. According to the DFT results, for the bioactive compounds in TCF, the E_{HOMO} value was negative, revealing that the physical adsorption is more probable than chemical adsorption. Physical adsorption has been described in various scientific articles as expressed as a negative E_{HOMO} [1,8,30].

The modeling and calculation results show that the ΔE, IP, and EA values are 0.08, 0.28, and 0.19 eV, respectively. The smaller HOMO–LUMO energy gap (ΔE = 0.08) indicates that electron donation from the inhibitor to the metal surface (reactive compound) is easier, which enhances its inhibitory ability. The calculated energy gap of moupinamide indicates favorable electronic properties for corrosion inhibition. A stronger synergistic effect of the inhibitor with the Fe metal corresponds with a reduced ΔE value[6]. The electron density distribution reveals that the nitrogen and oxygen atoms in the structure have significant electron donation abilities, which are essential for interacting with the metal surface[80]. In this work, the calculated energy gap of moupinamide suggests advantageous electronic characteristics for a corrosion inhibitor. The IP and EA values indicate that TCF can act as an electron donor and acceptor.

The computational and calculation results also confirmed that TCF has a lower chemical hardness (η, 0.23 eV) and tends to be soft (σ, 4.2 eV), indicating that the molecule is reactive and able to interact with metals. Chemical hardness (η) refers to the resistance of chemical species to polarization or deformation of electron clouds, where the inhibition efficiency is inversely proportional to the chemical hardness of a compound[89]. σ and η are essential factors that provide information regarding reactivity and stability, which could affect the efficacy of an inhibitor[19]. Soft molecules with small HOMO–LUMO energy gaps can be used as corrosion inhibitors because they have low HOMO–LUMO energy gaps[17]. In addition, ΔN denotes the release of electrons to the vacant orbital. The capacity of a chemical to inhibit is enhanced when its value is positive. The bioactive compound of TCF exhibited a positive value of 0.11, implying increased stability and chemical reactivity.

Based on the ΔE, σ, and η values, combined with the ΔN, it indicates that the TCF results are effective in reducing corrosion on carbon steel surfaces. Furthermore, the results of the electrostatic potential (ESP) map and ESP mesh tend to be evenly distributed throughout the molecule, with surrounding NaCl ions. The interaction with NaCl can slightly distort the geometry of the molecule, affect the electronic structure (HOMO/LUMO), and change its surface properties (ESP). These changes can affect the chemical behavior and interactions of moupinamide in the environment, which may be essential for further research on its potential use in developing science materials.

Conclusions

Tinospora cordifolia fraction (TCF) showed significant potential as an effective and sustainable corrosion inhibitor for carbon steel in a seawater environment, with the following key points of conclusion:

- Based on the HRMS and NMR analysis results, moupinamide in *Tinospora cordifolia* can be identified as an amide compound containing aromatic, amide (–CONH–), and methyl ($–CH_3$) groups.
- Electrochemical analysis confirmed that TCF effectively reduced the corrosion rate of carbon steel by forming a protective layer on the metal surface.
- Higher concentrations of TCF increase corrosion protection, as evidenced by increased R_{ct}, decreased I_{corr}, and increased *IE* on PDP and EIS.
- Increasing temperature tends to decrease the effectiveness of TCF as an inhibitor, as evidenced by a decrease in Rct, an increase in I_{corr}, and a reduced stability of the passive layer on EIS.
- The optimum inhibition efficiency was achieved at around 90.89% (PDP) and 92.25% (EIS) with the addition of 150 $mg.L^{-1}$ of TCF at 300 K.
- The inhibition mechanism is believed to involve the adsorption of bioactive compounds from *T. cordifolia* onto the carbon steel surface, forming a protective layer that prevents the penetration of corrosive substances from seawater media.
- Computational analysis using density functional theory (DFT) confirmed that the active compounds present in the TCF interact strongly with the carbon steel surface.

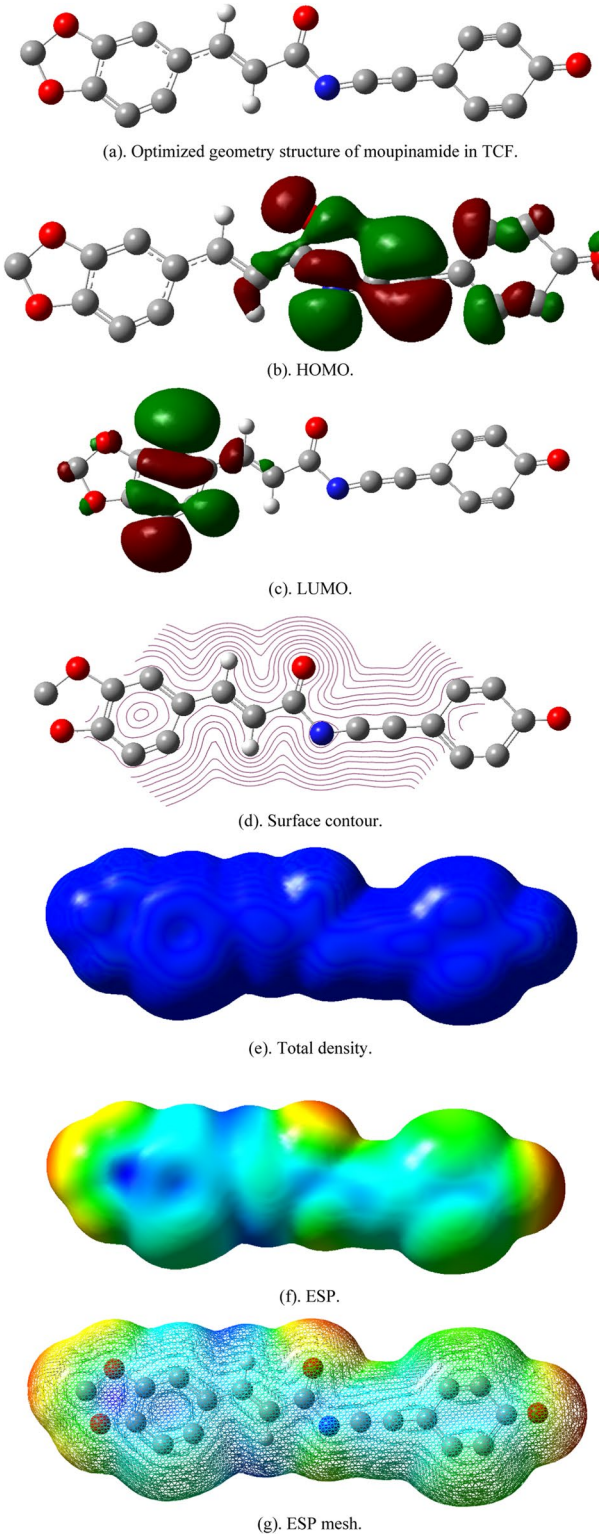

Fig. 15. Optimized geometry structure, HOMO, LUMO, surface contour, total density, and ESP for moupinamide from TCF in NaCl medium. The molecular structure and electronic properties were modeled using BIOVIA Materials Studio 2020 and GaussView 6.0.16 with the Dmol^3 module under GGA-PBE functional and DNP basis set. The HOMO and LUMO orbitals were localized mainly on the aromatic and amide functional groups, indicating high reactivity and interaction potential with carbon steel surfaces.

Code	Molecule
Basis set	DNP
Function	GGA
E_{HOMO} (ev)	−0.28076
E_{LUMO} (ev)	−0.19216
ΔE (eV)	0.0886
IP (eV)	0.28076
EA (eV)	0.19216
χ (eV)	0.0443
η (eV)	0.23646
σ	4.229045082
ΔN (Fe) (e)	0.107062911

Table 8. List of the parameters attained through the DFT analysis.

- Further studies are recommended to evaluate the long-term stability and performance of the inhibitor under different environmental conditions.

Received: 26 February 2025; Accepted: 2 September 2025
Published online: 05 October 2025

References

1. Mouats, N. et al. Comprehensive investigation of the adsorption, corrosion inhibitory properties, and quantum calculations for 2-(2,4,5-trimethoxybenzylidene) hydrazine carbothioamide in mitigating corrosion of XC38 carbon steel under HCl environment. *ACS Omega* **9**(26), 27945–27962. https://doi.org/10.1021/acsomega.3c10240 (2024).
2. Medupin, R. O., Ukoba, K. O., Yoro, K. O. & Jen, T. C. Sustainable approach for corrosion control in mild steel using plant-based inhibitors: A review. *Mater. Today Sustain.* **22**, 100373. https://doi.org/10.1016/j.mtsust.2023.100373 (2023).
3. Ochoa, N. et al. Modified cassava starches as potential corrosion inhibitors for sustainable development. *Mater. Res.* **16**(6), 1209–1219. https://doi.org/10.1590/S1516-14392013005000126 (2013).
4. Benachour, N. et al. 3,4–Dimethoxy phenyl thiosemicarbazone as an effective corrosion inhibitor of copper under acidic solution: comprehensive experimental, characterization and theoretical investigations. *RSC Adv.* **14**(18), 12533–12555. https://doi.org/10.1039/d3ra08629a (2024).
5. Miralrio, A. & Vázquez, A. E. Plant extracts as green corrosion inhibitors for different metal surfaces and corrosive media: A review. *Processes* https://doi.org/10.3390/PR8080942 (2020).
6. Tan, B. et al. A novel corrosion inhibitor for copper in sulfuric acid media: Complexation of iodide ions with Benincasa Hispida leaf extract. *Colloids Surf. Physicochem. Eng. Asp.* **705**(135710), 1–17. https://doi.org/10.1016/j.colsurfa.2024.135710 (2025).
7. Jenifer, J., Saratha, R. & Brindha, T. Bioactive seaweed extracts: Sustainable solutions for corrosion protection. *J. Bio. Tribo-Corrosion* **10**(4), 1–9. https://doi.org/10.1007/s40735-024-00896-4 (2024).
8. Tan, B. et al. *Nepeta cataria L.* leaf extracts as eco–conscious corrosion inhibitor for copper in H2SO4 medium. *Colloids Surf. Physicochem. Eng. Asp.* **711**(136399), 1–16. https://doi.org/10.1016/j.colsurfa.2025.136399 (2025).
9. Jayakumar, S. et al. Aqueous black seed (*Nigellasativa L.*) extract-mediated corrosion inhibition in mild steel exposed to 3.5% NaCl: Effect of temperature, pH, time, and in situ analysis using atomic force microscopy. *Trans. Indian Inst. Met.* **77**(11), 3385–3396. https://doi.org/10.1007/s12666-024-03399-5 (2024).
10. Luo, X. et al. Synthesis of natural glucomannan derivative as a highly–efficient green inhibitor for mild steel in the simulated seawater. *J. Ind. Eng. Chem.* **124**, 132–146. https://doi.org/10.1016/j.jiec.2023.03.006 (2023).
11. Okuma, S. O., Ogagavwodia, E. O., Ajokperiniovo, V. E. & Emurotu, J. E. Performance of acetone extract of anthocleista grandiflora as a potential bioinhibitor on corrosion behavior of carbon steel in seawater environment. *Period. Polytech. Chem. Eng.* **68**(4), 597–608. https://doi.org/10.3311/ppch.37241 (2024).
12. Vorobyova, V. & Skiba, M. Mechanism of inhibitory action of fruit cake extracts as a new environmentally inhibitors of carbon steel corrosion. *Results Chem.* https://doi.org/10.1016/j.rechem.2024.101317 (2024).
13. Zakeri, A., Bahmani, E. & Aghdam, A. S. R. Plant extracts as sustainable and green corrosion inhibitors for protection of ferrous metals in corrosive media: A mini review. *Corros. Commun.* **5**, 25–38. https://doi.org/10.1016/j.corcom.2022.03.002 (2022).
14. Royani, A., Hanafi, M., Haldhar, R. & Manaf, A. Evaluation of Morinda citrifolia extract as sustainable inhibitor for mild steel in saline environment. *J. Eng. Res.* https://doi.org/10.1016/j.jer.2024.01.013 (2024).
15. Rana, M., Joshi, S. & Bhattarai, J. Extract of different plants of nepalese origin as green corrosion inhibitor for mild steel in 0.5 M NaCl solution. *Asian J. Chem.* **29**(8), 1757–1760 (2017).
16. Bonatti, R. S., Costa, D., Padilha, G. S., Bortolozo, A. D. & Osório, W. R. Drimia maritima as a new green inhibitor for Al-Si Alloy, SAE steel and pure Al samples in 0.5 M NaCl solution: Polarization and electrochemical impedance analyses. *Metals* https://doi.org/10.3390/met14101147 (2024).
17. Abdallah, M. et al. Natural parsley oil as a green and safe inhibitor for corrosion of X80 carbon steel in 0.5 M H2SO4solution: A chemical, electrochemical, DFT and MC simulation approach. *RSC Adv.* **12**(5), 2959–2971. https://doi.org/10.1039/d1ra08855f (2022).
18. Ilim, L., Hidayah, D., Yuliyanda, K., Pandiangan, D. & Simanjuntak, W. Sodium methoxide catalyzed preparation of nitrogen compounds from palm oil methyl esters as corrosion inhibitor. *Sci Technol Indones* https://doi.org/10.26554/sti.2024.9.1.113-119 (2024).
19. Brioua, S. et al. Enhancing corrosion resistance of XC38 steel using sulfur and nitrogen-containing phenyl thiosemicarbazone: A comprehensive experimental and computational analysis. *J. Taiwan Inst. Chem. Eng.* **165**(105718), 1–24. https://doi.org/10.1016/j.jtice.2024.105718 (2024).
20. Ikeuba, A. I. et al. A combined electrochemical and DFT investigation of ornidazole as a benign anti-corrosion agent for carbon steel materials in acidizing environments. *Results Mater.* https://doi.org/10.1016/j.rinma.2024.100542 (2024).
21. Royani, A. et al. The potential of *Tinospora cordifolia* extracts as antibacterial material against pseudomonas aeruginosa. *Trends Sci.* **20**(1), 1–13. https://doi.org/10.48048/tis.2023.3884 (2023).

22. Sharma, R., Sharma, R., Singh, R. R. & Kumari, A. Evaluation of biogenic zinc oxide nanoparticles from *Tinospora cordifolia* stem extract for photocatalytic, anti-microbial, and antifungal activities. *Mater. Chem. Phys.* https://doi.org/10.1016/j.matchemphys.2023.127382 (2023).
23. Singh, B., Nathawat, S. & Sharma, R. A. Ethnopharmacological and phytochemical attributes of Indian *Tinospora* species: A comprehensive review. *Arab. J. Chem.* **14**(10), 1–75. https://doi.org/10.1016/j.arabjc.2021.103381 (2021).
24. Singh, D. & Chaudhuri, P. K. Chemistry and pharmacology of *Tinospora cordifolia*. *Nat. Prod. Commun.* **12**(2), 299–308. https://doi.org/10.1177/1934578x1701200240 (2017).
25. Kaur, G., Prabhakar, P. K., Lal, U. R. & Suttee, A. Phytochemical and biological analysis of *Tinospora cordifolia*. *Int. J. Toxicol. Pharmacol. Res.* **8**(4), 297–305 (2016).
26. Hussin, M. H., Jain Kassim, M., Razali, N. N., Dahon, N. H. & Nasshorudin, D. The effect of *Tinospora crispa* extracts as a natural mild steel corrosion inhibitor in 1 M HCl solution. *Arab. J. Chem.* https://doi.org/10.1016/j.arabjc.2011.07.002 (2016).
27. Royani, A. et al. Enhancing the corrosion inhibition performance of *Tinospora cordifolia* extract using different fractions of methanol solvent on carbon steel corrosion in a seawater-simulated solution. *Appl. Surf. Sci. Adv.* **18**, 100465. https://doi.org/10.1016/j.apsadv.2023.100465 (2023).
28. Sajadi, G. S., Salmanian, F., Naghizade, R. & Hosseini, S. M. A. The inhibitive action of lemon verbena plant extract as an economical and eco-friendly corrosion inhibitor for mild steel in acidic solutions. *Int. J. Electrochem. Sci.* **19**(8), 100699. https://doi.org/10.1016/j.ijoes.2024.100699 (2024).
29. Askari, M. & Ghaffarinejad, A. Copper corrosion prevention in 3.5% NaCl solution by Spartium junceum petals extract as an eco-friendly bio-inhibitor: Kinetic and thermodynamic studies. *Anal. Sci.* **39**(12), 1967–1979. https://doi.org/10.1007/s44211-023-00407-4 (2023).
30. Bashir, S., Thakur, A., Lgaz, H., Chung, I. M. & Kumar, A. Corrosion inhibition performance of acarbose on mild steel corrosion in acidic medium: An experimental and computational study. *Arab. J. Sci. Eng.* **45**(6), 4773–4783. https://doi.org/10.1007/s13369-020-04514-6 (2020).
31. Kamaruzzaman, W. M. I. W. M. et al. Experimental, DFT and molecular dynamic simulation of Andrographis paniculata as corrosion inhibitor for mild steel in artificial seawater. *Mater. Chem. Phys.* https://doi.org/10.1016/j.matchemphys.2023.128642 (2024).
32. Mamudu, U., Santos, J. H., Umoren, S. A., Alnarabiji, M. S. & Lim, R. C. Investigations of corrosion inhibition of ethanolic extract of *Dillenia suffruticosa* leaves as a green corrosion inhibitor of mild steel in hydrochloric acid medium. *Corros. Commun.* **15**, 52–62. https://doi.org/10.1016/j.corcom.2023.10.005 (2024).
33. Sanmugarajah, V., Rajkumar, G. & Panambara, P. A. H. A Detail review on heart-leaved moonseed (*Tinospora cordifolia*) medicinal plant. *J. Trop. Pharm. Chem.* **6**(2), 1–13. https://doi.org/10.25026/jtpc.vxix.xxx1 (2022).
34. Zhu, X. & Wang, C. Corrosion inhibition performance of an environmentally friendly water–based nano–inhibitor. *Alex. Eng. J.* **70**, 495–501. https://doi.org/10.1016/j.aej.2023.03.013 (2023).
35. Alrefaee, S. H., Rhee, K. Y., Verma, C., Quraishi, M. A. & Ebenso, E. E. Challenges and advantages of using plant extract as inhibitors in modern corrosion inhibition systems: Recent advancements. *J. Mol. Liq.* **321**(114666), 1–14. https://doi.org/10.1016/j.molliq.2020.114666 (2021).
36. Cui, M., Wang, Z. & Wang, B. Survival strategies of mangrove (Ceriops tagal (perr.) C. B. Rob) and the inspired corrosion inhibitor. *Front. Mater.* **9**(June), 1–10. https://doi.org/10.3389/fmats.2022.879525 (2022).
37. Cherrad, S. et al. Cupressus arizonica fruit essential oil: A novel green inhibitor for acid corrosion of carbon steel: *Cupressus arizonica* fruit essential oil. *Arab. J. Chem.* **15**(6), 103849. https://doi.org/10.1016/j.arabjc.2022.103849 (2022).
38. Nam, N. D., Ha, P. T. N., Anh, H. T., Hoai, N. T. & Hien, P. V. Role of hydroxyl group in cerium hydroxycinnamate on corrosion inhibition of mild steel in 0.6 M NaCl solution. *J. Saudi Chem. Soc.* **23**(1), 30–42. https://doi.org/10.1016/j.jscs.2018.03.005 (2019).
39. Benzidia, B. et al. A combined experimental and theoretical study of green corrosion inhibition of bronze B66 in 3% NaCl solution by Aloe saponaria (syn. Aloe maculata) tannin extract. *Curr. Res. Green Sustain. Chem.* **5**(100299), 1–10. https://doi.org/10.1016/j.crgsc.2022.100299 (2022).
40. Nour El Houda, S., Amel, B. & Malika, F. Trifolium repens extracts as a green corrosion inhibitor for carbon steel in a 35% NaCl solution. *J. Taiwan Inst. Chem. Eng* https://doi.org/10.1016/j.jtice.2024.105771 (2024).
41. Ali, I. H., Idris, A. M. & Suliman, M. H. A. Evaluation of leaf and bark extracts of *Acacia tortilis* as corrosion inhibitors for mild steel in seawater: Experimental and studies. *Int. J. Electrochem. Sci.* **14**(7), 6404–6419. https://doi.org/10.20964/2019.07.10 (2019).
42. Fouda, A. E. A. S. et al. Carob fruit extract as naturally products corrosion inhibitor for copper-nickel alloys in brine solutions. *Sci. Rep.* **14**(1), 1–15. https://doi.org/10.1038/s41598-024-80589-7 (2024).
43. Ekere, I. E., Agboola, O., Fayomi, S. O. I., Ayeni, A. O. & Ayodeji, A. Investigation of corrosion inhibition by cassava leaf DNA on AISI 1015 low carbon steel in sodium chloride solution. *Int. J. Corros. Scale Inhib.* **12**(2), 424–437. https://doi.org/10.17675/2305-6894-2023-12-2-3 (2023).
44. Benzidia, B., Barbouchi, M., Hammouch, H., Erramli, H. & Hajjaji, N. The exploitation of Aloe saponaria (syn. *Aloe maculata*) as a potential green corrosion inhibitor for bronze in a neutral chloride environment. *Biointerface Res. Appl. Chem.* **13**(5), 1–11. https://doi.org/10.33263/BRIAC135.439 (2023).
45. Ikhmal, W. M. K. W. M., Maria, M. F. M., Rafizah, W. A. W., Norsani, W. N. W. M. & Sabri, M. G. M. Corrosion inhibition of mild steel in seawater through green approach using *leucaena leucocephala* leaves extract. *Int. J. Corros. Scale Inhib.* **8**(3), 628–643. https://doi.org/10.17675/2305-6894-2019-8-3-12 (2019).
46. Sobhi, N. E. H., Boukhouiete, A., Foudia, M. & Benidir, S. Study on the performance of green corrosion inhibitor in protection of API 5L X60 in seawater environment. *Rev. Roum. Chim.* **68**(7–8), 383–389. https://doi.org/10.33224/rrch.2023.68.7-8.07 (2023).
47. Hamood, A. F. et al. Weight loss, electrochemical measurements and DFT studies on corrosion inhibition by 7-mercapto-4-methylcoumarin. *Results Eng.* https://doi.org/10.1016/j.rineng.2024.102677 (2024).
48. Tan, B. et al. N, S-carbon quantum dots as inhibitor in pickling process of heat exchangers for enhanced performance in multi-stage flash seawater desalination. *Desalination* **589**(117969), 1–15. https://doi.org/10.1016/j.desal.2024.117969 (2024).
49. Othman, N. K., Yahya, S. & Ismail, M. C. Corrosion inhibition of steel in 3.5% NaCl by rice straw extract. *J. Ind. Eng. Chem.* **70**, 299–310. https://doi.org/10.1016/j.jiec.2018.10.030 (2019).
50. Sanni, O., Ren, J. & Jen, T. C. Examining the ability of palm kernel shell extract to control corrosion and assess its economic value on thermo-mechanically treated steel in artificial seawater: a sustainable and environmentally friendly approach. *Front. Chem.* **12**(May), 1–19. https://doi.org/10.3389/fchem.2024.1396565 (2024).
51. Peng, L. et al. Inhibition effect of Triphenylmethane dyes for the corrosion of carbon steel in CO2-saturated NaCl corrosion Medium. *Materials* https://doi.org/10.3390/ma17051094 (2024).
52. A. A. Al-Asadi, A. S. Abdullah, N. I. Khaled, and R. J. M. Alkhafaja, "Effect of an Aloe Vera As a Natural Inhibitor on The Corrosion of Mild Steel in 1 wt. % NaCl," *Int. Res. J. Eng. Technol.*, vol. 2, no. 6, pp. 604–607, 2015
53. Veedu, K. K., Mohan, S., Somappa, S. B. & Gopalan, N. K. Eco-friendly anticorrosive epoxy coating from ixora leaf extract: A promising solution for steel protection in marine environment. *J. Clean. Prod.* https://doi.org/10.1016/j.jclepro.2022.130750 (2022).
54. Dehghani, A., Mostafatabar, A. H. & Ramezanzadeh, B. Synergistic anticorrosion effect of *Brassica Hirta* phytoconstituents and cerium ions on mild steel in saline media: Surface and electrochemical evaluations. *Colloids Surf.Physicochem. Eng. Asp* https://doi.org/10.1016/j.colsurfa.2022.130503 (2023).

55. Haddadi, S. A., Alibakhshi, E., Bahlakeh, G., Ramezanzadeh, B. & Mahdavian, M. A detailed atomic level computational and electrochemical exploration of the Juglans regia green fruit shell extract as a sustainable and highly efficient green corrosion inhibitor for mild steel in 3.5 wt% NaCl solution. *J. Mol. Liq.* **284**, 682–699. https://doi.org/10.1016/j.molliq.2019.04.045 (2019).
56. Mofidabadi, A. H. J., Dehghani, A. & Ramezanzadeh, B. Investigating the effectiveness of watermelon extract-zinc ions for steel alloy corrosion mitigation in sodium chloride solution. *J. Mol. Liq* https://doi.org/10.1016/j.molliq.2021.117086 (2022).
57. Timoudan, N. et al. Corrosion inhibition performance of benzimidazole derivatives for protection of carbon steel in hydrochloric acid solution. *RSC Adv.* **14**(41), 30295–30316. https://doi.org/10.1039/d4ra05070c (2024).
58. Nikolaychuk, P. A. et al. The inhibitory properties of the ambroxol derivative on the corrosion of mild steel in hydrochloric acid medium. *Int. J. Corros.* https://doi.org/10.1155/2024/2302202 (2024).
59. El-Maksoud, S. A. A., El-Dossoki, F. I., Abd-Elhamed, M. & Farag, A. A. Some new synthesized gemini cationic surfactants as corrosion inhibitors for carbon steel in hydrochloric acid solution. *J. Bio. Tribo-Corrosion* **9**(4), 1–16. https://doi.org/10.1007/s40735-023-00787-0 (2023).
60. Amadi, N. M. et al. 1-Hexadecyl-3-methylimidazolium tetrachloroindate ionic liquid as corrosion inhibitor for mild steel: Insight from experimental, computational, multivariate statistics and multi-quadratic regression based machine learning model. *Results Eng.* https://doi.org/10.1016/j.rineng.2024.103115 (2024).
61. Chidiebere, M. A., Anadebe, V. C. & Barik, R. C. Insight into the corrosion resistance of mild steel in an acidic environment in the presence of an organic extract: Experimental and computational approach. *Results Eng.* https://doi.org/10.1016/j.rineng.2024.102787 (2024).
62. Z. Y. Hu *et al.*, 2024 A novel fluorescent-tagged polycarboxylic scale inhibitor : design , synthesis and application 3, 1751–1776 https://doi.org/10.17675/2305-6894-2024-13-3-24.
63. Rehioui, M. et al. Development of a promising nontoxic corrosion inhibitor based on *Opuntia dillenii* seed oil for iron corrosion in 3Wt% NaCl: Experimental and theoretical approaches. *Chem. Data Collect.* **46**, 101037. https://doi.org/10.1016/j.cdc.2023.101037 (2023).
64. Muthukrishnan, P., Jeyaprabha, B. & Prakash, P. Adsorption and corrosion inhibiting behavior of *Lannea coromandelica* leaf extract on mild steel corrosion. *Arab. J. Chem.* **10**, S2343–S2354. https://doi.org/10.1016/j.arabjc.2013.08.011 (2017).
65. Kamran, M., Shah, A. U. H. A., Rahman, G. & Bilal, S. Potential impacts of prunus domestica based natural gum on physicochemical properties of polyaniline for corrosion inhibition of mild and stainless steel. *Polymers* https://doi.org/10.3390/polym14153116 (2022).
66. Zeino, A., Abdulazeez, I., Khaled, M., Jawich, M. W. & Obot, I. B. Mechanistic study of polyaspartic acid (PASP) as eco-friendly corrosion inhibitor on mild steel in 3% NaCl aerated solution. *J. Mol. Liq.* **250**, 50–62. https://doi.org/10.1016/j.molliq.2017.11.160 (2018).
67. Radi, M. et al. Performance of avocado seeds as new green corrosion inhibitor for 7075–T6 Al alloy in a 35% NaCl solution: Electrochemical thermodynamic, surface and theoretical investigations. *Port. Electrochim. Acta* https://doi.org/10.4152/pea.2023410603 (2024).
68. Fouda, A. S., Ahmed, A. M., El-Darier, S. M. & Ibrahim, I. M. Moringa oleifera as an eco-friendly corrosion inhibitor for carbon steel in hydrochloric acid solution. *Int. J. Corros. Scale Inhib.* **9**(4), 1630–1647. https://doi.org/10.17675/2305-6894-2020-9-4-27 (2020).
69. Tang, H. et al. In-depth insight into corrosion inhibition performance of sweet potato leaf extract as a green and efficient inhibitor for 6N01 Al alloy in the seawater: Experimental and theoretical perspectives. *Langmuir* **40**(18), 9543–9555. https://doi.org/10.1021/acs.langmuir.4c00148 (2024).
70. Alaneme, K. K., Olusegun, S. J. & Adelowo, O. T. Corrosion inhibition and adsorption mechanism studies of Hunteria umbellata seed husk extracts on mild steel immersed in acidic solutions. *Alex. Eng. J.* **55**(1), 673–681. https://doi.org/10.1016/j.aej.2015.10.009 (2016).
71. Honarvar Nazari, M., Shihab, M. S., Havens, E. A. & Shi, X. Mechanism of corrosion protection in chloride solution by an apple–based green inhibitor: Experimental and theoretical studies. *J. Infrastruct. Preserv. Resil.* https://doi.org/10.1186/s43065-020-00007-w (2020).
72. Ahanotu, C. C. et al. Pterocarpus santalinoides leaves extract as a sustainable and potent inhibitor for low carbon steel in a simulated pickling medium. *Chem. Pharm. Sustain* https://doi.org/10.1016/j.scp.2019.100196 (2020).
73. Marzaq, A. et al. Environmentally-friendly imidazolium-derived ionic liquid as a corrosion inhibitor for carbon steel in 1 M HCl: experimental and theoretical approach. *J. Dispers. Sci. Technol.S* https://doi.org/10.1080/01932691.2025.2520873 (2025).
74. Royani, A. et al. Unveiling green corrosion inhibitor of Aloe vera extracts for API 5L steel in seawater environment. *Sci. Rep.* **14**(1), 1–20. https://doi.org/10.1038/s41598-024-64715-z (2024).
75. Dávila, J. et al. Bidens pilosa extract as a corrosion inhibitor on 1008 carbon steel in neutral medium. *J. Electrochem. Sci. Eng.* **14**(3), 321–338. https://doi.org/10.5599/jese.2331 (2024).
76. Mitrović, M. et al. Dandelion (*Taraxacum officinale*) root extract as a green corrosion inhibitor of steel in 3% NaCl. *Period. Polytech. Chem. Eng.* **68**(4), 609–619. https://doi.org/10.3311/PPch.37211 (2024).
77. Ezzat, A. O., Aigbodion, V. S., Al-Lohedan, H. A. & Ozoude, C. J. Unveiling the corrosion inhibition efficacy and stability of silver nanoparticles synthesized using Anacardium occidentale leaf extract for mild steel in a simulated seawater solution. *RSC Adv.* **14**(26), 18395–18405. https://doi.org/10.1039/d4ra02362e (2024).
78. Zlatić, G. et al. Green inhibition of corrosion of aluminium alloy 5083 by *Artemisia annua L.* extract in artificial seawater. *Molecules* https://doi.org/10.3390/molecules28072898 (2023).
79. Vorobyova, V. & Skiba, M. Peach pomace extract as novel cost-effective and high-performance green inhibitor for mild steel corrosion in NaCl solution: Experimental and theoretical research. *Waste Biomass Valoriz.* **12**(8), 4623–4641. https://doi.org/10.1007/s12649-020-01333-6 (2021).
80. Palaniappan, N. et al. Experimental and DFT studies on the ultrasonic energy-assisted extraction of the phytochemicals of: Catharanthus roseus as green corrosion inhibitors for mild steel in NaCl medium. *RSC Adv.* https://doi.org/10.1039/c9ra08971c (2020).
81. Alibakhshi, E. et al. Persian Liquorice extract as a highly efficient sustainable corrosion inhibitor for mild steel in sodium chloride solution. *J. Clean. Prod.* **210**, 660–672. https://doi.org/10.1016/j.jclepro.2018.11.053 (2019).
82. Loto, R. T. & Loto, C. A. Synergistic combination effect of green organic derivatives on the corrosion inhibition of mild steel in simulated seawater. *Orient. J. Chem.* **34**(4), 1802–1809. https://doi.org/10.13005/ojc/3404013 (2018).
83. Abd El-Lateef, H. M. et al. Novel natural surfactant-based fatty acids and their corrosion-inhibitive characteristics for carbon steel-induced sweet corrosion: Detailed practical and computational explorations. *Mater. Front.* https://doi.org/10.3389/fmats.2022.843438 (2022).
84. Zhou, Z. et al. A novel green corrosion inhibitor extracted from waste feverfew root for carbon steel in H2SO4 solution. *Results Eng.* https://doi.org/10.1016/j.rineng.2023.100971 (2023).
85. Hashim, N. Z. N. et al. XPS and DFT investigations of corrosion inhibition of substituted benzylidene Schiff bases on mild steel in hydrochloric acid. *Appl. Surf. Sci.* **476**, 861–877. https://doi.org/10.1016/j.apsusc.2019.01.149 (2019).
86. Yamashita, T. & Hayes, P. Analysis of XPS spectra of Fe 2+ and Fe 3+ ions in oxide materials. *Appl. Surf. Sci.* **254**(8), 2441–2449. https://doi.org/10.1016/j.apsusc.2007.09.063 (2008).

87. Ferkous, H. et al. A comparative study of novel synthesized sulfamide compounds: Electrochemical, morphological, XPS, and theoretical investigations on copper corrosion inhibition in 1.0 M HCl. *J. Mol. Liq.* **394**(123781), 1–19. https://doi.org/10.1016/j.molliq.2023.123781 (2024).
88. Njoku, D. I. et al. Corrosion protection of Q235 steel in acidic-chloride media using seed extracts of Piper guineense. *J. Mol. Liq.* **330**, 115619. https://doi.org/10.1016/j.molliq.2021.115619 (2021).
89. Rehioui, M. et al. 1,2,4-triazole-5-thione derivative for inhibiting carbon steel corrosion in 1 M HCl: Synthesis, electrochemical, SEM/EDX, DFT, and MD investigations. *J. Mol. Struct.* **1303**, 137577. https://doi.org/10.1016/j.molstruc.2024.137577 (2024).

Acknowledgements
The author wishes to extend gratitude to the National Research and Innovation Agency (BRIN), especially the corrosion laboratory at the Research Centre for Metallurgy and the organic laboratory at the Research Centre for Chemistry, for providing facilities and infrastructural support. The Universitas Indonesia (The Directorate of Research and Development) supported this study through the "PUTI 2024 Research Grant" program, contract number NKB-387/UN2. RST/HKP.05.00/2024.

Author contributions
Ahmad Royani: conceptualization (main idea), methodology, Investigation, data curation, formal analysis, visualization, resources, writing-original draft, writing-review, and editing. Muhammad Hanaf: formal analysis, validation, writing review, and editing. Abhinay Thakur: computation, analysis, writing, review and editing. Abdelkader Zarrouk: validation, writing review, and editing. Nabisab Mujawar Mubarak: formal analysis, validation, writing-review & editing. Azwar Manaf: conceptualization, writing, review, and editing, supervision. All authors declare and agree that Ahmad Royani is the main contributor to this paper, and all authors have given their approval.

Declarations

Competing interests
The authors declare no competing interests.

Statement of Identification
The specimen of *T. cordifolia* used in this study was identified by Dr. Ir. Hendro Wicaksono, M.Sc., Eng and deposited in the Herbarium Bogoriense laboratory, Directorate of Scientific Collection Management—BRIN, with ID letter B-1810/II.6.2/DI.05.07/6/2022.

Data availability
The corresponding author exhibits all of the information related to this work. All data or inquiries regarding this study can be obtained by contacting the corresponding author.

Additional information
Correspondence and requests for materials should be addressed to A.R., N.M.M. or A.M.

Reprints and permissions information is available at www.nature.com/reprints.

Publisher's note Springer Nature remains neutral with regard to jurisdictional claims in published maps and institutional affiliations.